ELSEVIER

Catalysis Today 23 (1995) 219–250

CATALYSIS TODAY

HREM study of the behaviour of a Rh/CeO_2 catalyst under high temperature reducing and oxidizing conditions

S. Bernal *, F.J. Botana, J.J. Calvino, G.A. Cifredo, J.A. Pérez-Omil, J.M. Pintado

Departamento de Ciencia de Materiales Ingeniería Metalúrgica y Química Inorgánica, Facultad de Ciencias, Universidad de Cádiz, Apartado 40, Puerto Real, 11510 Cádiz, Spain

Abstract

This work reports on the HREM study of a series of Rh/CeO_2 catalysts reduced at temperatures ranging from 623 to 1173 K. Computer simulation and digital processing techniques were also used to arrive at a finer interpretation of the experimental micrographs. Throughout the whole range of reduction temperatures, images in both profile and planar views show the existence of a well-defined structural relationship between metal and support. The profile imaging technique has allowed us to study the rhodium/ceria interface. It consists of Rh(111) in epitaxial relationship with (111) ceria surface planes. For the whole metal particle two different crystallographic orientations with respect to the support, both compatible with a $Rh(111)/CeO_2(111)$ interface, were observed. Metal decoration phenomena have also been found. They could only be observed on catalysts reduced at either 973 or 1173 K, the covering effects being much heavier in the latter case. The metal particle size distributions corresponding to the reduced catalysts show that metal sintering is slight up to 973 K, with mean sizes ranging from 3.5 to 3.7 nm, and much stronger when the catalysts are reduced at 1173 K, mean size: 6.7 nm. Reoxidation studies at 373, 523, 773 and 1173 K, have revealed that upon O_2 treatment at 773 K the metal particles thoroughly transform into Rh_2O_3, the precise structural nature of which could not be unequivocally established. These studies have also shown that for oxygen treatments up to 773 K, metal redispersion is rather modest, being necessary to heat to 1173 K to induce the spread of the oxidized rhodium phase onto the support and the subsequent redispersion. For the catalyst reduced at 1173 K, the reoxidation at 773 K or below does not lead to the recovery of the metal decoration effects. The ensemble of results presented here are discussed in relation to the nature of the metal/support interaction phenomena occurring in Rh/CeO_2 catalysts. The influence of both the reduction and reoxidation treatments on the metal deactivation/regeneration of these catalysts is also discussed.

1. Introduction

For the past few years, many laboratories all over the world have been working on ceria supported metal catalysts [1–36]. The intrinsic scientific interest of M/CeO_2 catalytic systems, as well as their close relationship with the so-called 'three-way catalysts' (TWC's) [37–40] would explain such an intense research activity around them.

It is generally acknowledged that chemisorption techniques cannot be applied in the conventional way for characterizing M/CeO_2 catalysts [3,4,7,20,25,47]. Several reasons justify this statement. First, bare ceria can strongly chemisorb the most usual probe molecules like H_2 [41–43] or CO [44–46]. Second, it is known that, in the presence of highly dispersed rhodium, at room temperature, large amounts of hydrogen can be transferred from the metal to the ceria support [20,21,25,47]. Some recent studies from our lab-

* Corresponding author.

SSDI 0920-5861(94)00165-0

oratory [22,47] have shown, however, that the spillover contribution to the total amount of hydrogen chemisorbed on Rh/CeO_2 catalysts, is sensitive to the specific reduction/evacuation conditions used for preparing them. Moreover, there are some clear indications in the sense that the chlorine from the metal precursor salts can strongly modify the structural nature of the support [10,48,49] as well as the chemisorptive properties of the M/CeO_2 catalysts [47,50,51]. In brief, no simple straightforward interpretation of the conventional chemisorption measurements seems to be possible in the case of M/CeO_2 catalysts. This has led to the development of alternative specific procedures like low-temperature (191 K) hydrogen chemisorption [22,47], which has been fruitfully used to estimate metal dispersions in Rh/CeO_2 catalysts, or the quantitative measurement of the ν_{CO} band intensity applied for characterizing Pt/CeO_2 catalysts [3,4].

It is also worth recalling, because of the acknowledged reducibility of ceria [42, 43,52,53], that M/CeO_2 catalysts have been considered as a model system exhibiting some kind of strong metal/support interaction phenomena [26]. This may induce further perturbations on their chemisorptive and catalytic properties.

In their theoretical model [26], Sánchez and Gázquez have suggested the existence of significant differences between the metal/support interaction occurring on M/TiO_2 catalysts, for which they reserve the term SMSI effect, and the strong metal/support interaction phenomena exhibited by oxide supports with fluorite-like structure, as is the case of CeO_2. For titania supported metal catalysts, the onset of the SMSI effect is considered to occur at reduction temperatures higher than 673 K, 773 K being very commonly used to induce the SMSI state [58,59]. In accordance with [58,59], the SMSI effect is characterized by a number of features, the most commonly accepted being: strong inhibition of the metal chemisorptive capabilities against the classic probe molecules like H_2; occurrence of metal decoration effects; strong disturbance of the catalytic behaviour; reversibility of the phenomenon by reoxidation and further reduction at milder temperatures. Very recently, a detailed NMR study of the hydrogen interaction with Rh/TiO_2 has quite convincingly shown that both geometric and electronic effects have a significant contribution to the SMSI effect [60]. This proposal is also consistent with the chemisorption and HREM studies reported in ref. [61] for Rh/TiO_2 under the SMSI state. In accordance with [61], partial covering of the metal crystallites could only be observed, but complete inhibition of their capability for H_2 chemisorption did occur.

From the experimental point of view, many authors have reported the occurrence of peculiar metal/support interaction phenomena on ceria supported metal catalysts [2,7,11,14,18,26,27, 31,34,47,54–57]. There are, however, notable uncertainties about the precise nature of this interaction. Some authors [7,11,12,56,62] have suggested that metal/ceria interaction can be described in terms of the so-called SMSI effect. Their conclusion was mainly based on chemisorption and/or catalytic activity studies. In some cases [7], though metal decoration effects are suggested to occur, no direct proof of it could be provided. Moreover, the authors [7] acknowledge the existence of significant differences between their Rh/CeO_2 catalysts reduced at 773 K and Rh/TiO_2 under SMSI state. Thus, no strong inhibition of the hydrogen chemisorption capability could be observed upon high temperature (773 K) reduction [7]. This latter observation has also been reported for several different Rh/CeO_2 samples [22,47], as well as on Pt/CeO_2 catalysts [54], all of them reduced with H_2 at 773 K. In these latter cases [22,47,54], the occurrence of metal/support interaction phenomena other than the classic SMSI effect are suggested to occur. The same conclusion is arrived at in ref. [34].

It is often suggested that transmission electron microscopy can hardly be used to characterize ceria supported metal catalysts [3,4]. In fact, when the resolution limit of the microscope prevents its use in the phase contrast mode, and the operation in the diffraction contrast mode is necessary, the strong dispersive power of cerium

makes it difficult to characterize a metal phase highly dispersed on CeO_2. This is true, even in the case of heavy metals like platinum [3,34]. It is worth noting, however, that some earlier studies from the literature clearly show that high resolution electron microscopy [14,18,19,47,61,63,64] constitutes a very powerful tool to investigate the nanostructural nature of M/CeO_2 catalysts. Likewise, TEM, STEM and microdiffraction techniques have been used fruitfully to characterize ceria-containing multicomponent metal catalysts [27,34,65–67]. Though the number of electron microscopy studies at present available is rather limited, some very important information concerning the microstructural nature of these catalysts have already been discovered. First, data concerning the metal particle size could be obtained [18,47]. This provides an essential reference for the chemisorption studies. Second, HREM images for M/CeO_2 (M: Pt, Au, Rh) catalysts have shown the occurrence of a quite characteristic epitaxial relationship [14,27,47,61, 63,64]. Third, the electron microscopy studies reported to date have not provided any evidence of metal decoration effects on M/CeO_2 catalysts [14,18,19,27,34,47,61,63]. In the case of titania supported metal catalysts, this effect has clearly been shown by using high resolution electron microscopy [61,68,69].

It is important to note, that a very large majority of the studies commented on above have dealt with M/CeO_2 catalysts reduced at 773 K or lower temperatures. This represents an important limitation because, as far as the understanding of the catalytic behaviour and deactivation mechanisms in TWC's is concerned, the investigation should be extended to a wider temperature range. In accordance with this, we have developed a research project aimed at studying the microstructural evolution of Rh/CeO_2 catalysts when treated under both high temperature reducing and oxidizing conditions. In the present work, high resolution electron microscopy combined with computer simulation and digital processing techniques will be used with two major objectives: (1) To investigate further the nature of the metal/support interaction phenomena occurring in Rh/CeO_2 catalysts reduced in a wide range of temperatures up to 1173 K. (2) To investigate the effect of the reduction temperature as well as of the reoxidation treatments on the particle size distribution and mean particle size of the rhodium-containing phase. All these studies are in close connection with the investigation of the deactivation mechanisms operating in ceria supported metal catalysts and by extent in three-way catalysts. In accordance with very recent literature [70–72], deactivation is a major problem in TWC's.

2. Experimental

The Rh/CeO_2 catalysts studied in this work were prepared by the incipient wetness impregnation technique from an aqueous solution of $Rh(NO_3)_3$. The ceria used, with a purity of 99.9%, was a low surface area sample from Alpha Ventron. After the impregnation treatment, the sample was dried in air, at 383 K, for 10 h, and further stored in a dessicator until its reduction. This impregnation/drying cycle was repeated several times up to a final metal loading of 2.4% by weight was reached. As determined from N_2 adsorption at 77 K, the BET surface area of the catalysts was 11 $m^2\ g^{-1}$. This value did not change with the reduction temperature, except for the sample reduced at 1173 K. In this latter case, some catalyst sintering could be observed.

The reduction treatments were carried out by heating the $Rh(NO_3)_3/CeO_2$ precursor system in a flow of H_2 (60 $cm^3\ min^{-1}$), from 298 K to the selected reduction temperature (623, 773, 973 or 1173 K). The heating rate was 10 K min^{-1}. The samples were held for 1 h at the reduction temperature, then they were treated in flowing He (60 $cm^3\ min^{-1}$), for 1 h, at the reduction temperature, and finally they were cooled, also in a flow of inert gas. In the particular case of the catalyst reduced at 623 K, the heating in a flow of He following the reduction treatment was performed at 773 K. In this way, we ensure the complete elimination of

Table 1
Lattice spacings and angles for CeO_2 and Rh in [110], [111] and [100] orientations

Zone axis	Planes	Angles between planes	CeO_2 d_{hkl} (nm)	Rh d_{hkl} (nm)
⟨001⟩	{220}	45° with {200}	0.191	0.135
	{200}	90° with {200}	0.271	0.190
		45° with {220}		
⟨110⟩	{220}	90° with {200}	0.191	0.135
	{200}	90° with {220}	0.271	0.190
	{111}	70.5° with {111}	0.312	0.220
		54.7° with {200}		
		35.3° with {220}		
⟨111⟩	{220}	60° with {220}	0.191	0.135

CeO_2: fluorite structure (space group: Fm3m); a_0: 0.541 nm.
Rh: fcc structure (space group: Fm3m); a_0: 0.380 nm.

the hydrogen chemisorbed on ceria [22]. To prevent the fast reoxidation of the reduced catalysts, they were cooled to 191 K, always in a flow of He, then treated with O_2 (5%)/He for 0.5 h, warmed up to 295 K in the oxidizing mixture, and finally exposed to air. The samples prepared in this way were rapidly transferred into the microscope following the procedure reported elsewhere [18].

The HREM images were obtained on a JEOL-2000-EX microscope with 0.21 nm point-resolution. The instrument was equipped with a top-entry specimen holder and an ion pump. The computer-simulated HREM images were obtained by running the EMS software package on an IRIS 4D35/TG+ silicon graphics workstation. The digital processing of both calculated and experimental HREM images was performed on a digital microcomputer, PC-AT-486. The experimental images were digitalized on a high resolution monochrome CCD camera, COHU, model 4910. The whole digital processing was performed with the help of the SEMPER 6+ software package.

Two computer programs developed at the University of Cádiz (UCA) have also been routinely used in this work. They were written in FORTRAN 77. The so-called EJE Z Program was designed to establish the zone axis of a known structure allowing to obtain HREM images on a microscope of a specific resolution. The RHODIUS program has allowed us to build up the supercell structural models used as the bases for the computer simulations presented in this work. When applied to the simulation of supported metal systems, the size and shape of the metal crystallites can be controlled at will. Likewise, it allows to define the crystallographic and chemical nature of the metal/support interface.

3. Results and discussion

3.1. HREM study of metal/support interaction phenomena in Rh/CeO_2 catalysts

A major goal of this work is to show the very interesting possibilities of the HREM technique as a tool for investigating the metal/support interaction phenomena in M/CeO_2 catalysts. In the present case, we shall focus our attention on the rhodium/ceria system.

Two main aspects will be considered below. On the one hand, we shall study the nature of the metal/support structural relationships observed in Rh/CeO_2 catalysts. On the other hand, we shall

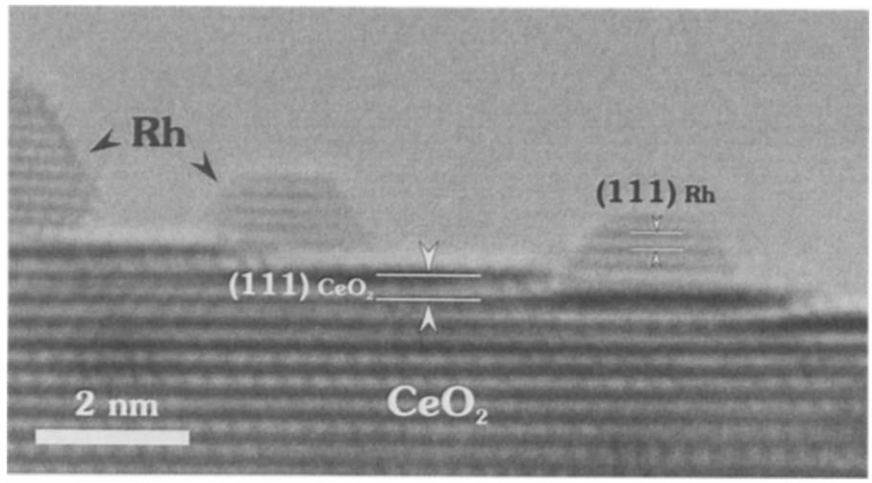

Fig. 1. HREM image in profile view of Rh/CeO_2 reduced at 623 K.

investigate the metal decoration phenomena observed to occur on them. The first effect has been detected throughout the whole range of reduction temperatures, from 623 to 1173 K. In contrast with this, the covering of the metal particles by the support could only be observed at the highest reduction temperatures: 973 K, and much more heavily on the catalyst reduced at 1173 K. As will be shown in the next sections of this work, the HREM technique can help to clarify some fundamental questions about these two manifestations of the metal/support interaction phenomena occurring in Rh/CeO_2 catalysts.

3.1.1. HREM study of the structural relationships observed on Rh/CeO_2 catalysts

3.1.1.1. Application of HREM profile imaging techniques. From nanodiffraction studies carried out on Rh/CeO_2 catalysts reduced at either 623 or 773 K, Pan et al. [27] have reported the existence of a well-defined structural relationship between ceria and the rhodium crystallites sitting on it. It is shown in ref. [27] that such a structural relationship consists of the parallel alignment of metal and support [*hkl*] axes with the same Miller indexes. Specifically, they have reported experimental nanodiffraction patterns showing parallel orientations in [111] and [100] directions. From this observation, they suggest the occurrence of a Rh/CeO_2 epitaxial relationship consisting of the parallel growth of (*hkl*) planes of rhodium on (*hkl*) planes of the support. This type of structural relationship would also be consistent with the HREM images reported in refs. [47,64].

With the help of a computer program developed at UCA (EJE Z), we have established the zone axis allowing to obtain HREM images for ceria and rhodium crystals. Using a microscope with 0.21 nm point resolution, [110] direction is the only one fulfilling such a requirement for both, metal and support. Table 1 reports on the crystallographic data corresponding to Rh and CeO_2 in [110] orientation. Structural information concerning [111] and [100] orientations are also included for comparison.

Fig. 1 accounts for a HREM profile image corresponding to our Rh/CeO_2 catalyst reduced at 623 K. It clearly shows that (111) rhodium planes grow parallel to the (111) planes of ceria. As proposed earlier in refs. [27,47,64], this image suggests the epitaxial growth of the metal crystallites on the support. To gain some further insight into the nature of such a structural relationship, we have studied the crystallography of both metal and support surface planes exhibiting the highest atomic densities. Table 2 summarizes the results obtained from this study. Data for the Ce^{4+} and O^{2-} sublattices corresponding to {111} and {100} faces of ceria as well as for the same faces

Table 2
Crystallographic data for faces {111} and {100} of ceria and metallic rhodium

		Surface plane	Vector t_1 (nm)	Vector t_2 (nm)	Angle t_1/t_2	Density node·nm^{-2}
CeO_2	Ce^{4+}	{111}	3.82	3.82	60°	7.91
		{100}	3.82	3.82	90°	6.85
CeO_2	O^{2-}	{111}	3.82	3.82	60°	7.91
		{100}	2.70	2.70	90°	13.70
Rh		{111}	2.68	2.68	60°	16.04
		{100}	2.68	2.68	90°	13.89

of the fcc rhodium structure are included in Table 2.

It can be deduced from Table 2 that for (111) planes the ratio of metal to support surface lattice vectors $t_{111}(Rh):t_{111}(CeO_2)$ is 3:2 with approximately a 6% misfit. It can also be concluded from Table 2 that, consequently to the sixfold symmetry axis of these (111) planes, a 60° rotation of a (111) Rh plane parallel to a (111) ceria plane leads to an equivalent metal/support interface. Two different epitaxial relationships, both corresponding to a parallel orientation: Rh(111)// CeO_2(111), can therefore be considered. For 0° rotation, all the [*hkl*] axes of the metal and support are aligned, thus resulting in an epitaxial relationship of parallel axis. It will be referred to as Rh(111)//CeO_2(111) 0°. For 60° rotation, though [111] axes of the metal and support are parallel to each other, several others become misaligned. As a result, a nonequivalent crystallographic situation, hereafter referred to as Rh(111)//CeO_2 (111) 60°, can be found. Fig. 2, Fig. 3, Fig. 4 show structural models aimed at describing the two epitaxies mentioned above. Fig. 2 depicts a common model for the metal/support interface, whereas Figs. 3 and 4 show the profile view in [110] orientation for 60° and 0° epitaxial relationships, respectively. These two Rh/CeO_2 supercells were generated by using a computer program (RHODIUS) developed at the University of Cádiz. As will be discussed below, our experimental HREM images show that both possibilities do occur.

In accordance with the crystallographic data included in Table 2, the Rh(200)//CeO_2(200) epitaxy seems to be likely too. In fact, 45° rotation of the (200) Rh plane with respect to the (200) surface plane of ceria leads to an almost perfect fitting of the two surface structures, Fig. 5. In spite of this, we have not been able to find any experimental image corresponding to such an epitaxy. It must be noted, however, that, in our ceria support, (100) face is much less abundant than the (111).

The HREM technique of surface profile imaging is considered to be a powerful tool for investigating very fine details of catalyst surfaces [14,73]. By using this technique, the two structural relationships mentioned above: Rh(111)// CeO_2 (111) 60° (Fig. 6) and 0° (Fig. 7) could be observed. Fig. 6a shows a HREM experimental image for a rhodium microcrystal with truncated cuboctahedron shape sitting on ceria. Both metal and support are in [110] orientation. The interpretation of this image was also confirmed by computer simulation. Fig. 6b accounts for the calculated image. It was obtained by running the multislice routine of the EMS software package. The basis for the computer calculations was the structural model in Fig. 3. The simulation conditions were as follows. Metal crystal size: 3.2 nm; ceria support thickness: 9 nm; electron beam accelerating voltage: 200 kV; objective lense aperture

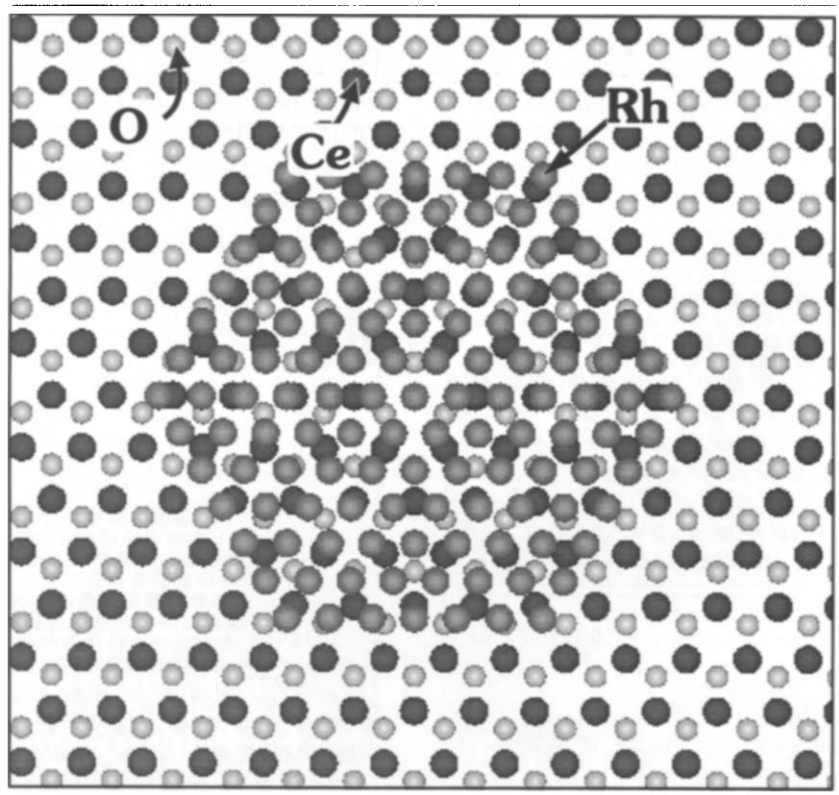

Fig. 2. Planar view of a Rh(111)/CeO_2(111) interface. Structural model generated by using the RHODIUS program.

diameter: 12 nm^{-1}; defocus spread: 10 nm; beam semiconvergence: 1.2 mrad; defocus, Δf: 50 nm; C_S: 0.7 mm.

Fig. 7a shows an edge-on HREM image corresponding to our Rh/CeO_2 catalyst reduced at 623 K. Both metal and support are close to the [110] orientation. As already discussed in ref. [47], this image shows the (111) planes of rhodium lying parallel to (111) ceria planes. Accordingly, it can be considered as representative of a (111)// (111) 0° epitaxial relationship. To confirm such a proposal, we have also recorded the corresponding computer-simulated images. The structural model on which the calculations were based is depicted in Fig. 4. The simulation conditions were the same as reported above for Fig. 6b. A series of calculated HREM images was obtained by rotating the whole metal/support supercell out of the [110] zone axis. Rotation angles ranging from 0° to 15° were considered here. Fig. 7b and c, depict the calculated images obtained for 7° and 0° rotation, respectively. As can be deduced from the comparison of the experimental and calculated images, Fig. 7a and b are quite similar to each other, thus indicating that the experimental one (Fig. 7a) was recorded slightly out of zone.

A further aspect worth commenting on is the mechanism of accommodation between the rhodium and ceria lattices. Because the difference of lattice parameters, no perfect matching between metal and support (111) planes can occur. Accordingly, a rather peculiar interface can be observed in Fig. 7a.

The experimental HREM image in Fig. 7a was further studied with the help of digital processing techniques. In this way, an intensity profile along the line crossing the rhodium crystallite from one lateral face to the other could be recorded. Fig. 8 accounts for the intensity variations throughout this line. The distance between successive peaks allows the measurement of the rhodium lattice spacing in the microcrystal. It can be noted, how-

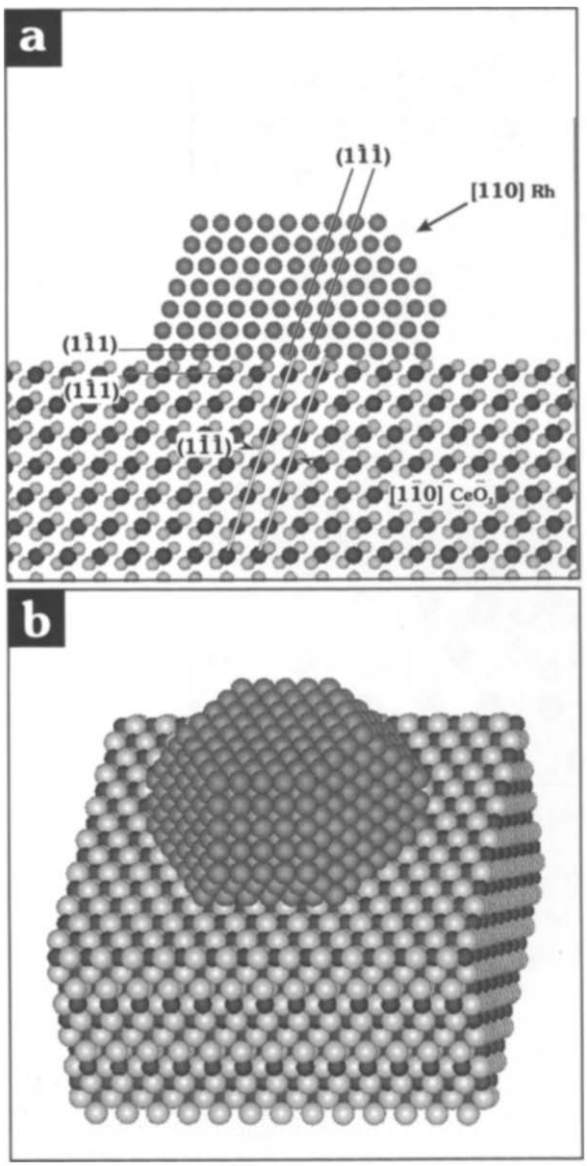

Fig. 3. Truncated cuboctahedral rhodium crystallite epitaxially grown on ceria. Epitaxial relationship: Rh(111)/CeO_2(111) 0°. Views along the [001] (a) and [431] (b) directions of the whole metal/support supercell. Structural model generated by using the RHODIUS program.

ever, that the intrinsic accuracy of this measurement (1 pixel: 0.01 nm) does not permit a precise estimate of specific spacings. Instead, a mean value was determined by dividing the distance between lateral faces by the whole number of spacings. This procedure has already been used in ref. [74]. The average value was found to be 0.226 nm. Because of the small size of the metal particle in Fig. 7a, the spots corresponding to (111) Rh planes in the reciprocal space image were rather diffuse. Under these circumstances, the accuracy of the lattice spacing value determined from it was a little bit worse than that estimated from measurements on the real space image.

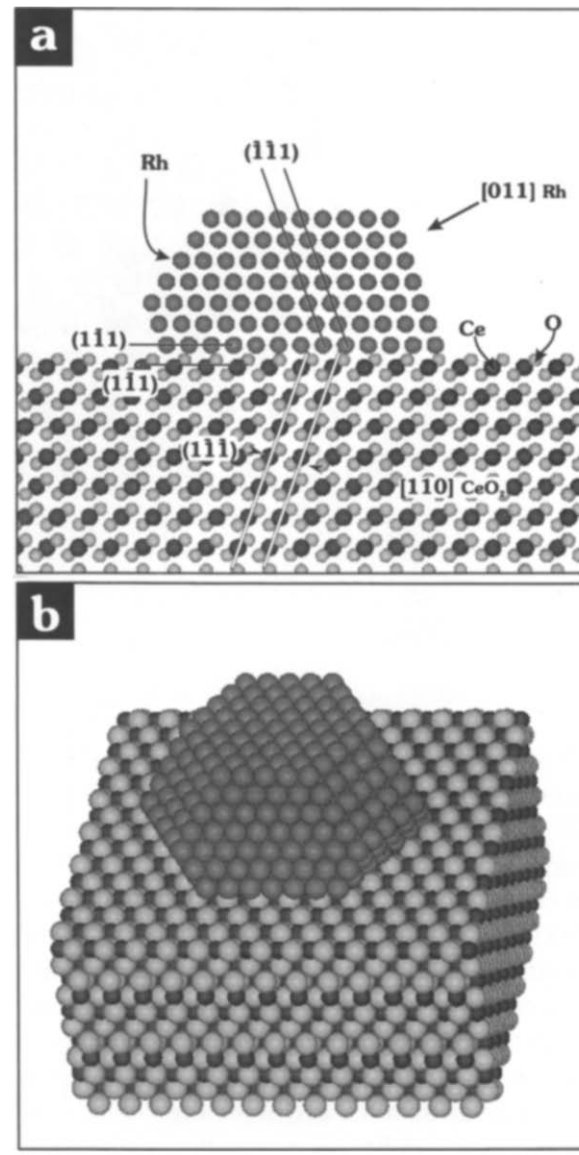

Fig. 4. Truncated cuboctahedral rhodium crystallite epitaxially grown on ceria. Type of epitaxy: Rh(111)/CeO_2(111) 60°. Views along the [001] (a) and [431] (b) directions of the whole metal/support supercell. Structural model generated by using the RHODIUS program.

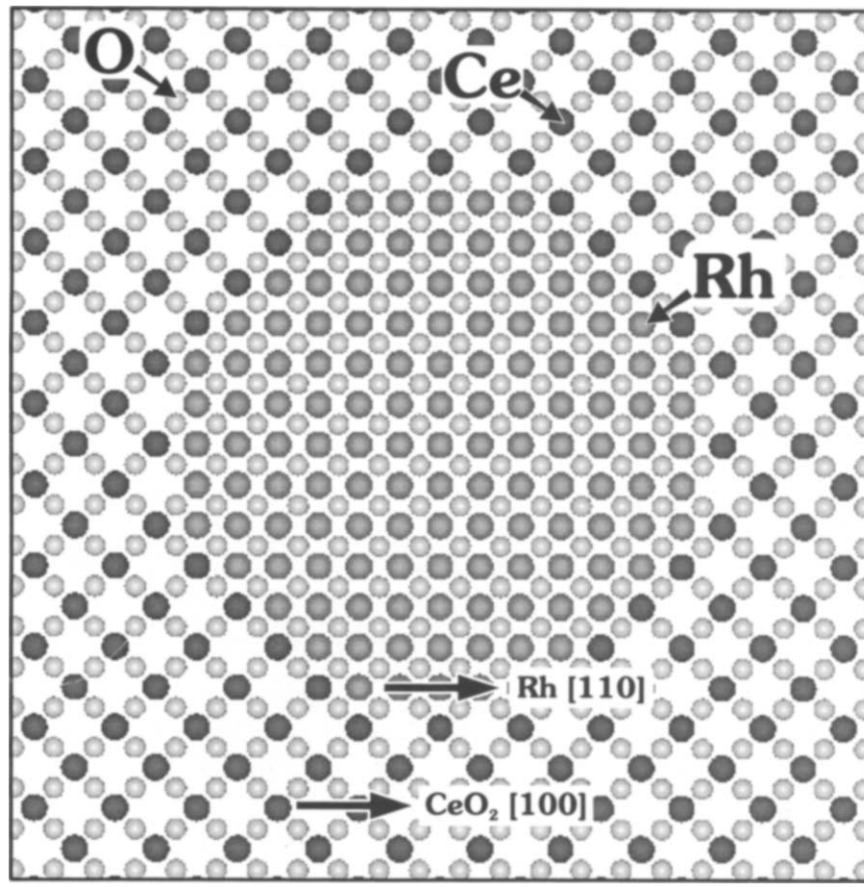

Fig. 5. Planar view of a Rh(100)/CeO_2(100) interface. Structural model generated by using the RHODIUS program.

If it is taken into account that the (111) lattice spacing for bulk rhodium is 0.220 nm, our estimation above would represent a slight expansion of the metal lattice (3.5%). A parallel study carried out on the simulated image in Fig. 7b led to a mean spacing of 0.224 nm. It can be noted, however, that the structural model used to generate the calculated image does not assume any distortion of the rhodium lattice. Therefore, it cannot be excluded that, at least for relatively small metal particles, part of the observed expansion can be due to an optical artifact. In summary, the intrinsic accuracy of our measurement as well as the results obtained for the simulated image oblige us to take the expansion of the rhodium lattice with some reserve. In this respect, it must also be noted that similar measurements carried out on a much larger rhodium crystallite, Fig. 9, indicate a negligible distortion of the (111) metal lattice spacing.

The analysis of the contrasts observed at the rhodium/ceria interface in Figs. 7a, 7b and 9, deserve some further comments. First of all, as indicated on Fig. 9, there seems to be a sequence of contrasts which is repeated regularly. It consists of 7 (111) rhodium planes matching 5 (111) ceria planes. The same sequence can also be found in Fig. 7a for a much smaller metal particle. This would lead to a lattice misfit of 1.8%. The precise meaning of such contrasts is unclear. It could be thought that they are due to local distortions induced by the interaction with ceria. However, this interpretation does not seem to be confirmed by computer simulations, because, as deduced from Fig. 7b, rather similar contrasts are observed

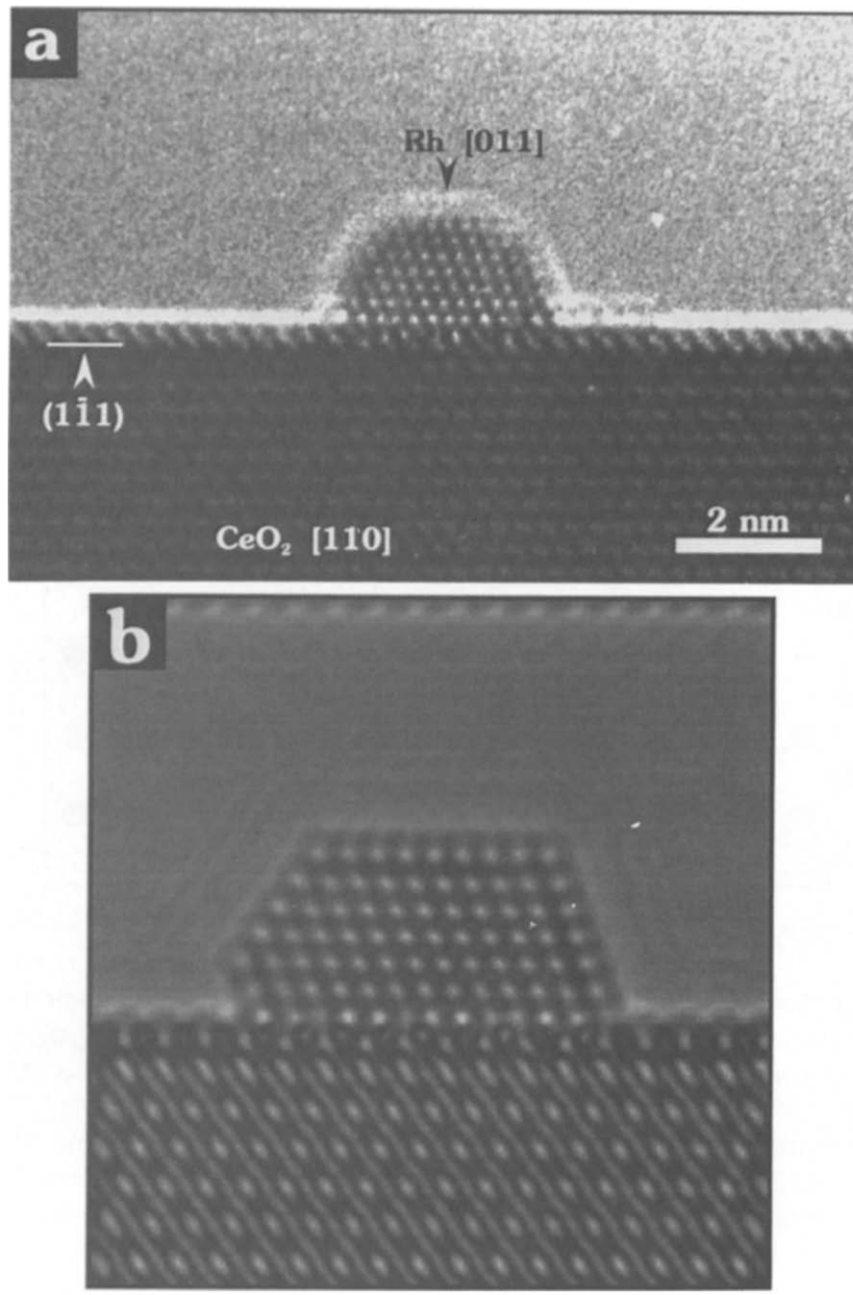

Fig. 6. HREM study of Rh/CeO_2. Experimental (a) and computer simulated (b) profile images of a metal particle showing a Rh(111)/CeO_2(111) 60° epitaxial relationship.

on the simulated image, for which, as mentioned above, no rhodium distortion has been considered.

There is a second aspect worth commenting on concerning the contrasts at the rhodium/ceria interface in Fig. 7a. Instead of being flat, this interface shows a seesaw shape. This poses some interesting questions about the nature of the metal/support interaction in this type of catalyst. It should be recalled that, in accordance with ref. [26], the strong metal/support interaction in M/CeO_2 catalysts consists in the anchoring of the metal crystallites to the surface support. Sánchez

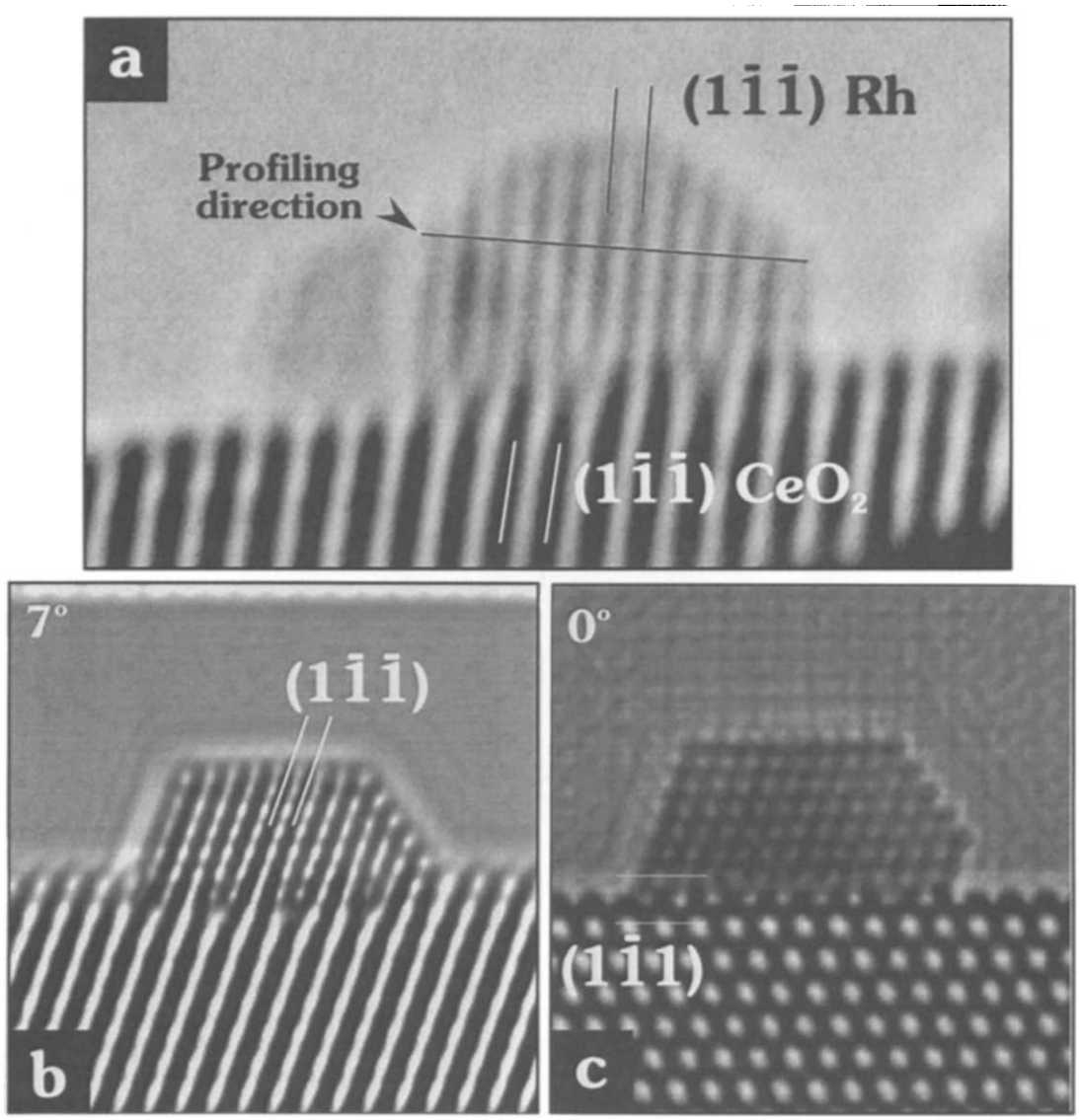

Fig. 7. HREM study of the Rh(111)/CeO_2(111) 0° epitaxial relationship. Experimental micrograph corresponding to the Rh/CeO_2 catalyst reduced at 623 K (a). Simulated images of the metal/support system in [110] orientation (c) and 7° out of the [110] zone axis (b).

and Gázquez [26] suggest that the fixation of the metal particles takes place through what they call a 'nesting' process, by the virtue of which metal atoms occupy the anionic vacancies created at the support surface. A HREM image like that reported in Fig. 7a might tentatively be interpreted in terms of the occurrence of a nesting phenomenon. A comparison of the experimental image (Fig. 7a) with the simulated one (Fig. 7b) is helpful in this respect. In effect, we notice on the calculated image the same type of contrasts observed in Fig. 7a. However, as deduced from Fig. 4, the structural model used to generate the image in Fig. 7b assumes a flat Rh(111)/CeO_2(111) interface, i.e. no nesting effect has been considered. This implies that, though Sánchez et al.'s model should not be disregarded, it is not possible to intuitively interpret Fig. 7a in terms of such a model.

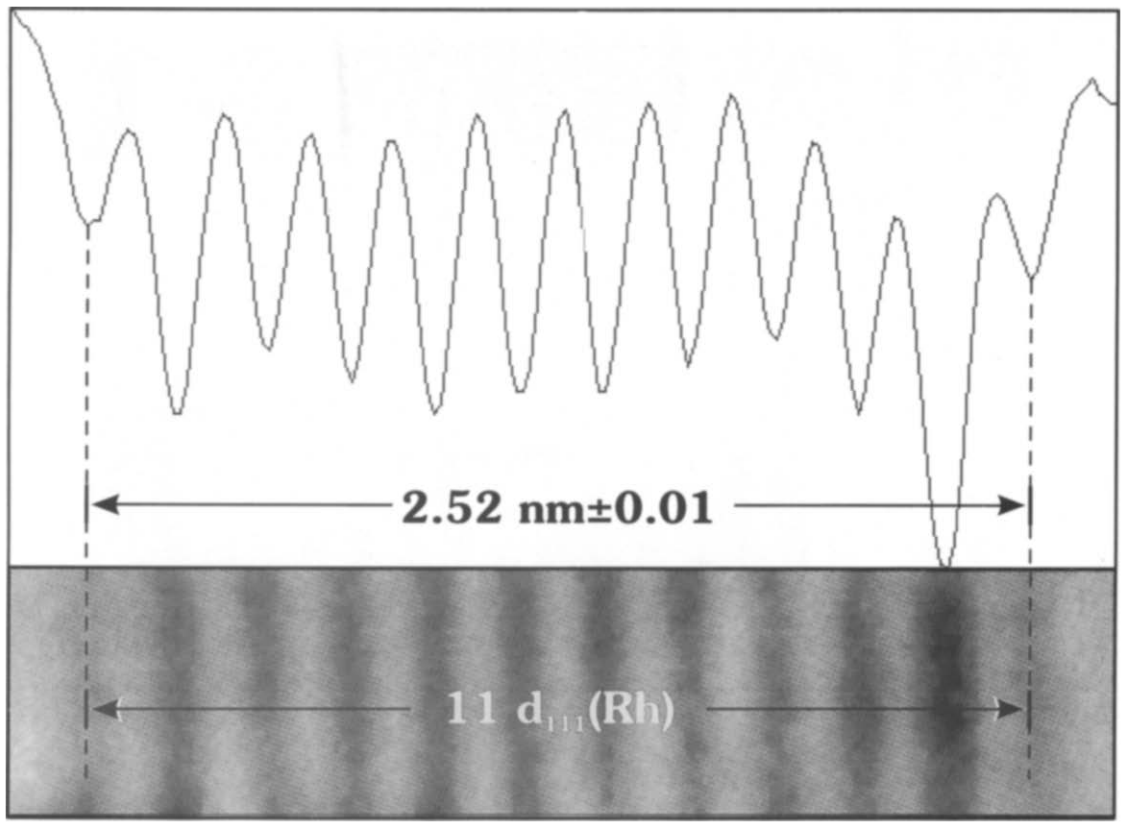

Fig. 8. Application of digital processing techniques to the estimation of the Rh(111) fringe spacing in Rh/CeO_2. Intensity profile along the line crossing the metal particle in Fig. 7a.

3.1.1.2. HREM study of the Rh/CeO_2 system in planar view. Moiré patterns. The HREM images for metal crystallites in planar projection on the support can also provide some useful information about the structural relationships in Rh/CeO_2 catalysts. The analysis of these images shows the frequent occurrence of Moiré fringes in parallel alignment with those of the support (Fig. 10). This is generally interpreted as an indication of a parallel orientation between the two overlapping lattices [75]. It is also well known that the existence of a simple relationship between the spacing of the Moiré pattern and those of the superimposed lattices are responsible for it. In the case of a Moiré pattern generated from first order reflections [76]:

$$e = d_1 d_2 / (d_1^2 + d_2^2 - 2 d_1 d_2 \cos\theta)^{1/2} \quad (1)$$

where e, d_1 and d_2 stand for the fringe spacings of the Moiré pattern and overlapping crystal lattices respectively; and θ accounts for the angle between these lattices, 0° in the present case.

With the help of digital processing techniques, we have measured the spacings corresponding to both the Moiré patterns and the support fringes in the surrounding region. These measurements were made in the reciprocal space. From them, the metal and support crystal orientations were established, and the corresponding metal fringe spacing could be estimated. The analysis of the Moiré patterns can thus constitute an alternative way of detecting variations in the metal lattice parameters. This would be particularly useful when the lattice parameters of the metal to be investigated are below the resolution limit of the microscope.

Fig. 11b and d account for the optical diffraction pattern (ODP) obtained by digital processing of

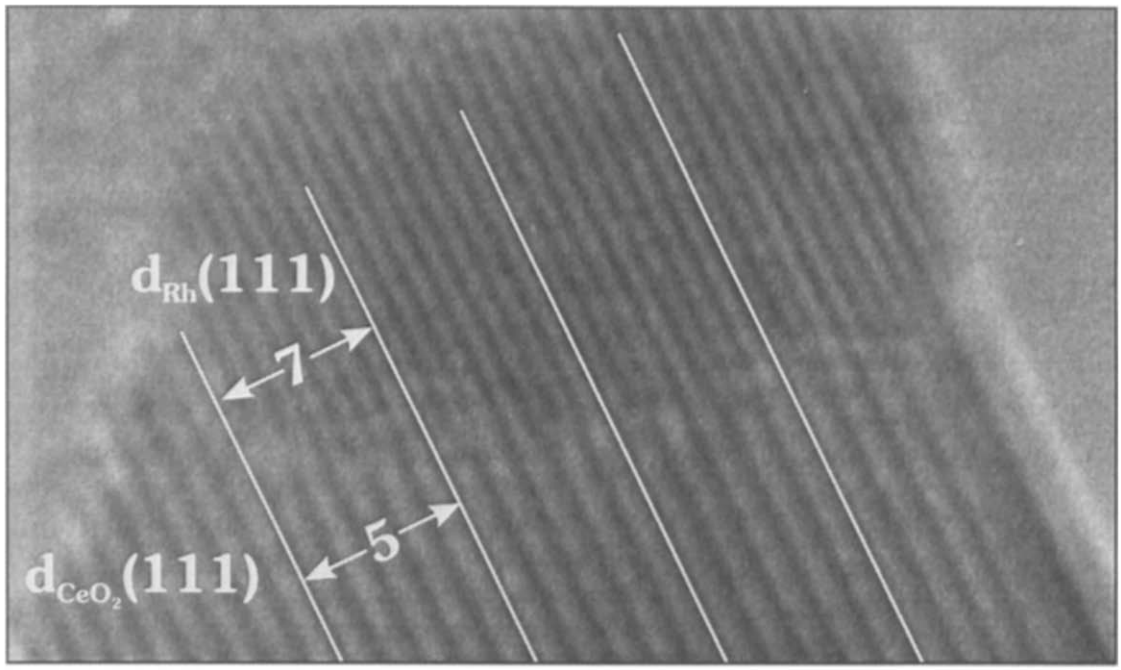

Fig. 9. HREM study of the metal/support interface. Epitaxial relationship Rh(111)/CeO_2(111) 0°. Experimental image corresponding to the catalyst reduced at 973 K.

the experimental images in Fig. 11a and c, respectively. In the case of the Moiré pattern recorded along the [110] direction, Fig. 11a, the ODP shows that the spots corresponding to (111) planes of CeO_2 are oriented in the same direction just beyond those of the Moiré pattern, Fig. 11b, thus indicating a parallel alignment of metal and support (111) planes. For the Moiré pattern recorded in [100] orientation, Fig. 11c, the ODP in Fig. 11d clearly shows that (200) reflections of ceria and rhodium are involved in the double diffraction process. The fringe spacing for the Moiré patterns could also be determined. In the case of Rh(111)//CeO_2(111) parallel orientations, they were found to range from 0.740 nm to 0.840 nm. Accordingly, by using Eq. (1), (111) fringe spacings for rhodium ranging from 0.219 to 0.227 nm could be estimated. The accuracy of this estimate was ± 0.008 nm. As already deduced from the digital processing of Figs. 7a and 9, the study of the Moiré patterns suggests that the (111) lattice spacings for Rh, though variable from one metal particle to the other, are often slightly larger than those corresponding to the massive metal. However, the accuracy of the measurements does not make it possible to draw a fully significant conclusion about this effect.

In some cases, the experimental HREM images of the rhodium crystallites sitting in planar view on ceria show the absence of the expected Moiré pattern. Fig. 12 shows an ensemble of rhodium crystallites with their [111] axis parallel to the [111] orientation of ceria. Some of them do exhibit Moiré fringes, whereas some others do not. As confirmed by the corresponding ODP's, the encircled metal particles in Fig. 12 account, respectively, for the two situations mentioned above. To find out the origin of such an observation, we have carried out a computer simulation of the HREM images resulting from a metal crystallite projected on the ceria surface, both in [110] orientation. We have considered the two epitaxial relationships Rh(111)//CeO_2(111) 60° as well as 0°. Fig. 13b and d account, respectively, for these two epitaxies. The computer calculations were performed on the basis of the structural models included, respectively, in Fig. 13a and c. For the sake of clarity, these supercell models are

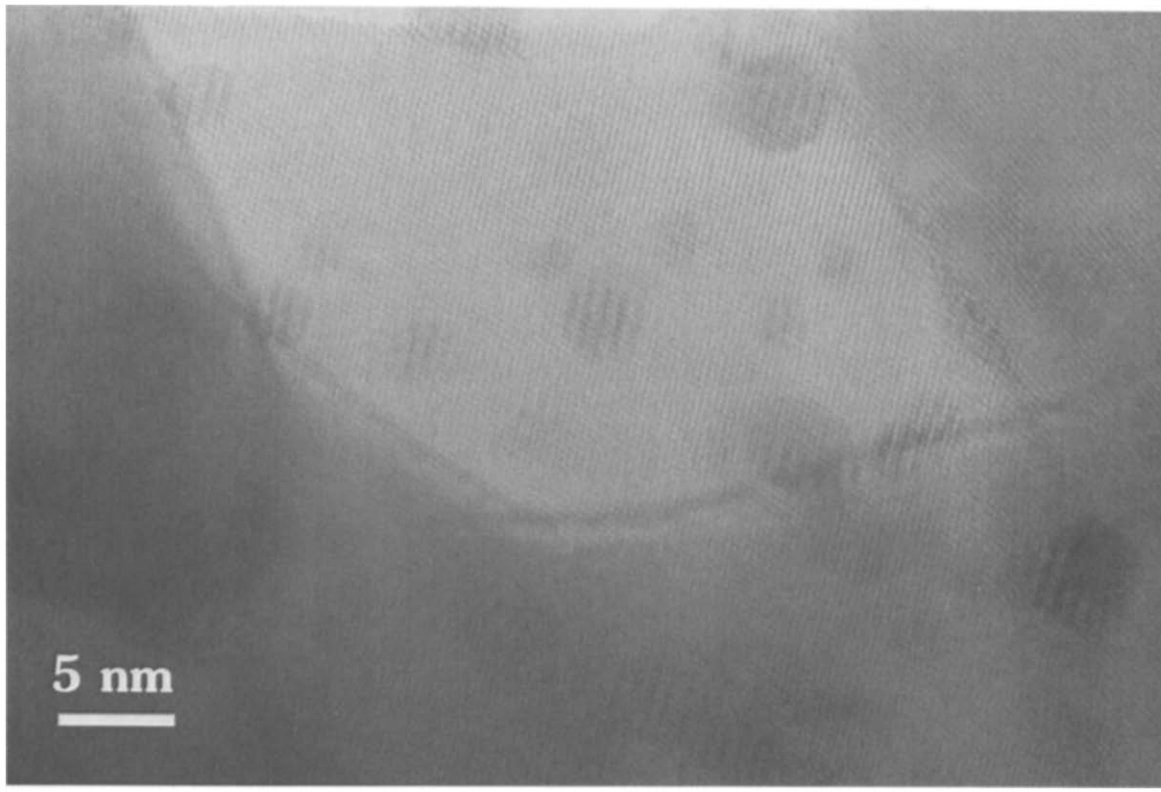

Fig. 10. HREM image for rhodium crystallites in planar projection on ceria. Metal and support [111] axes are in parallel orientation. Zone axis [110]. Sample reduced at 1173 K.

shown in profile view. The simulation conditions were as follows. Rhodium particle size: 6 nm; ceria thickness: 9 nm; zone axis: [110]. The electronoptical conditions were the same used in the computer calculations reported above.

The analysis of the calculated images in Fig. 13 leads to the conclusion that the Moiré pattern can only be observed for the epitaxy of parallel axes (0° rotation). The simulation shown in Fig. 13d corresponds to a bidimensional Moiré pattern, which is very seldom observed in the experimental images. Accordingly, we have also included in Fig. 13e a calculated image based on model c, but slightly tilted (5°) out of zone. This latter image accounts fairly well for the experimental ones. Since the profile imaging technique has shown that most of the metal crystallites are epitaxially oriented with respect to the support, it can reasonably be concluded that the planar view HREM images not showing Moiré fringes are due to the Rh(111)//CeO_2(111) (60° rotation) epitaxy. In other words, the analysis of the Moiré patterns would also allow us to distinguish the two types of Rh(111)//CeO_2(111) epitaxial relationships described here.

As shown in Fig. 11c, we have also found experimental Moiré patterns due to a double diffraction effect occurring on rhodium and ceria crystals with their (100) planes in parallel orientation. Though this finding might well be considered as an indication of the occurrence of a Rh(100)// CeO_2(100) epitaxial relationship, it does not prove it. In effect, the observation of a parallel alignment of [100] metal and support directions does not mean that the metal/support interface is made up of (100) planes. In fact, as already mentioned, the so-called Rh(111)//CeO_2 (111) 0° epitaxy implies that all the metal and support planes with the same (*hkl*) Miller indexes are parallel to each other.

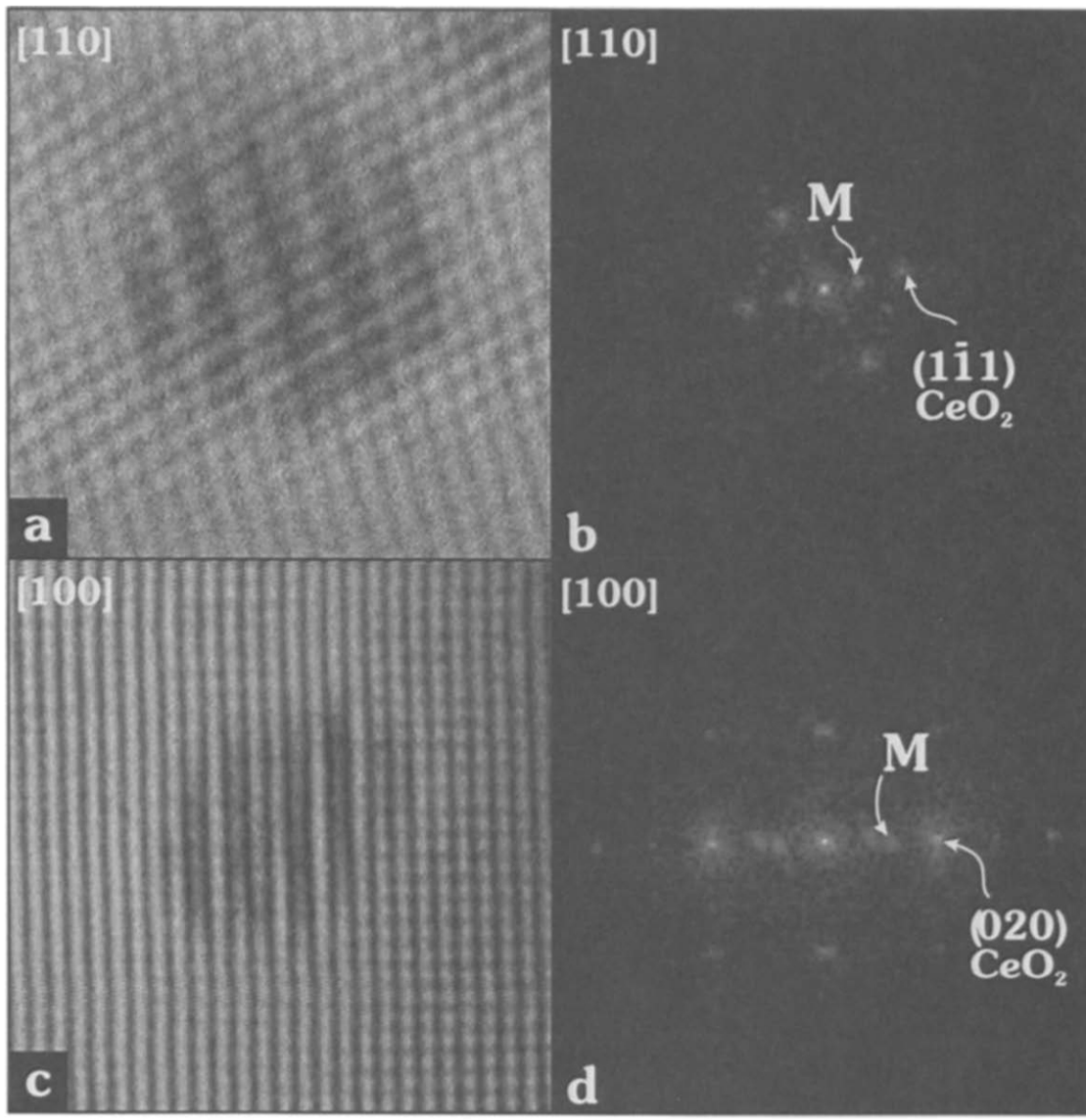

Fig. 11. Experimental Moiré diffraction patterns generated by Rh microcrystals in parallel orientation with CeO_2. (a) Rh(111)//CeO_2(111), catalyst reduced at 1173 K. (c) Rh(100)//CeO_2(100), catalyst reduced at 773 K. Spots marked with M on the ODP's (b) and (d) correspond to the Moiré pattern.

3.1.2. HREM study of the metal decoration effects in Rh/CeO_2: catalysts reduced at high temperatures

All the HREM profile images recorded for Rh/CeO_2 reduced at 773 K or lower temperatures show clean and well-faceted metal crystallites. This observation fully agrees with all the HREM studies on ceria supported metal catalysts which have appeared to date [14,18,19,47,61,63,64]. It is important to note that in all these references the reduction temperature was not higher than 773 K. In contrast with this, the reduction of our Rh/CeO_2 at either 973 or 1173 K induces significant changes on the microstructure of the metal crystallites. Fig. 14 and Fig. 15 show micrographs recorded for catalysts reduced, respectively, at 973 and 1173 K. Some new contrasts can be observed in the borders of the rhodium particles, the contours of which become less sharply defined. This can be interpreted as being due to

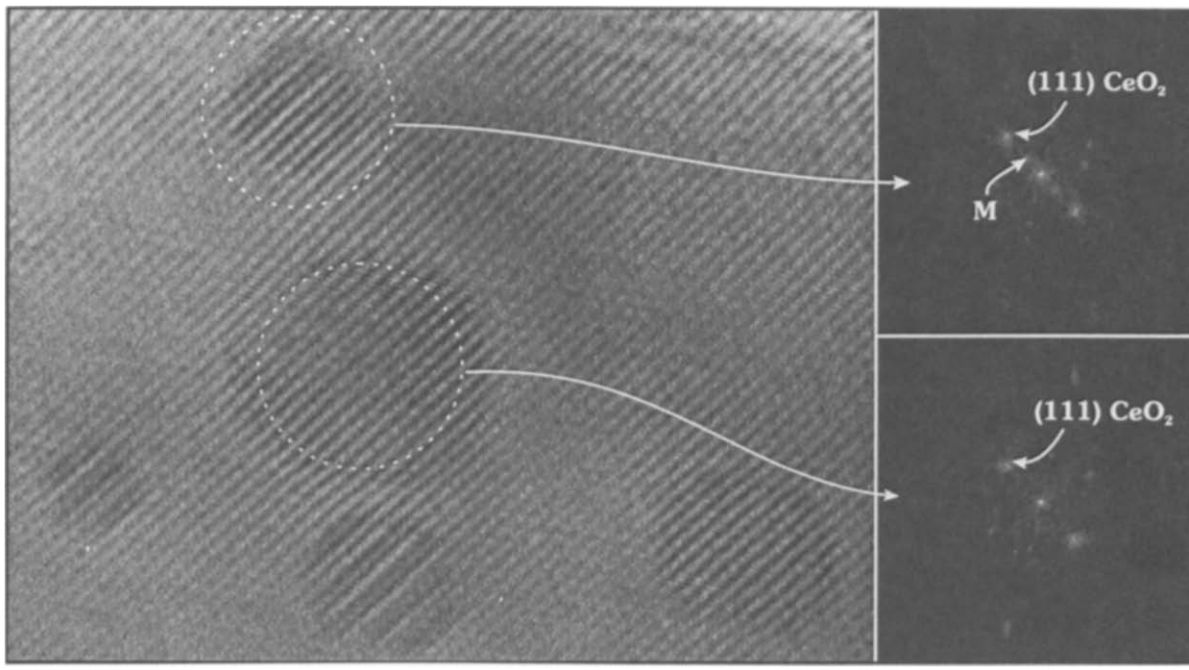

Fig. 12. HREM image of Rh crystallites in planar projection on ceria. Catalyst reduced at 1173 K. [111] axes of metal and support are in parallel orientation. Notice that some of the metal particles show Moiré fringes, others do not.

the occurrence of some covering of the metal crystallites by a different phase.

It has also been observed that the frequency of the decorated rhodium crystallites is much higher in the case of the catalyst reduced at 1173 K. An approximate statistical analysis suggests that no more than 30% of the metal particles appear decorated in the case of the catalyst reduced at 973 K, whereas over 90% of rhodium is covered in the case of the sample reduced at the highest temperature. The analysis of the ensemble of micrographs recorded for high temperature reduced catalysts also suggests that for the sample reduced at 1173 K the phase covering the metal particles is thicker and more crystalline. From all this evidence, we conclude that the onset of the decoration effect must occur at reduction temperatures close to 973 K; and therefore, that the complete absence of such a phenomenon on Rh/CeO_2 catalysts reduced at 773 K would be very reasonable.

To get some further insight into the nature of the metal covering phenomena reported here, we have carried out a specific study on the decorated rhodium particles. Computer simulation and digital processing techniques were also applied in this study. The latter technique was used to estimate fringe spacings of the phase covering the rhodium crystallite in Fig. 16a. A value of 0.31 nm could be measured, thus indicating that it consists of ceria support. There are some other points to be commented on. Fig. 16a and c shows two experimental HREM images of a focal series recorded for the catalyst reduced at 1173 K. It can be deduced from them that, upon modifying the focalization, either the metal crystallite (Fig. 16c) or the covering phase (Fig. 16a) can be clearly observed. By using the supercell model of the decorated metal particle included in Fig. 16e, we have simulated a focal series, two images of which are reported in Fig. 16b and d. In accordance with the experimental observations noted in the previous sections, the model assumes that the ceria planes covering the metal are in epitaxial relationship with rhodium. As in the case of the experimental micrographs, the calculated images show that upon varying Δf from 50 nm to 70 nm the contrasts at the metal particle change from a situation where the rhodium crystallite can hardly be

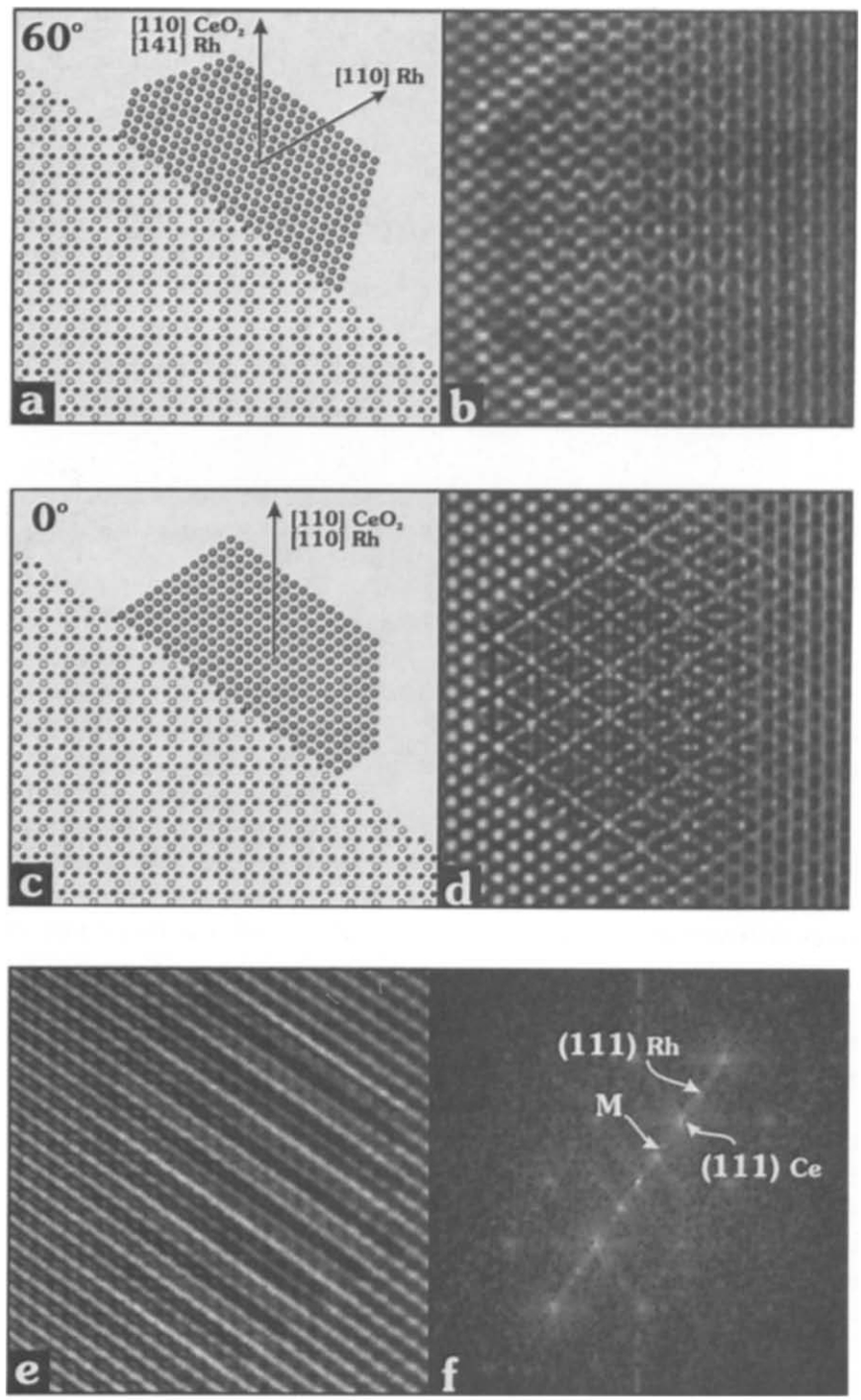

Fig. 13. Simulated HREM images for a rhodium crystallite in planar projection on ceria. The zone axis is parallel to the [110] direction of CeO_2. Models of the Rh(111)/CeO_2(111) 60° (a) and Rh(111)/CeO_2 0° (c) epitaxial relationships were used for generating images (b) and (d), respectively. Image (e) was calculated from model (c) by tilting the whole metal/support supercell 5° out of the zone axis.

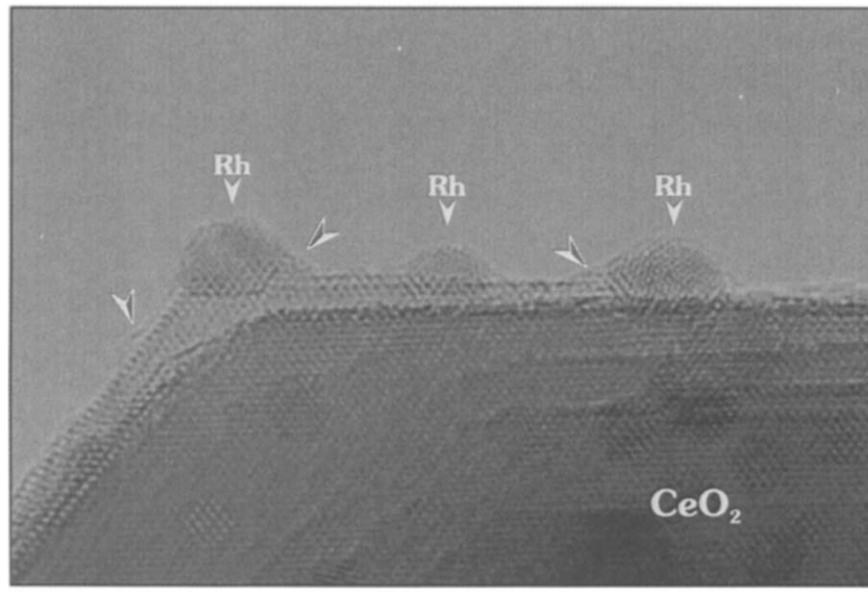

Fig. 14. HREM image of Rh/CeO_2 reduced at 973 K. Notice the occurrence of metal covered by the support.

observed to another one where metal fringes are well resolved.

Also worth noting is that the experimental images in Fig. 16 strongly suggest that metal decoration takes place by virtue of a process consisting of the support migration on top of the metal crystallite, rather than the penetration of the rhodium particle into the support. This is in agreement with the suggestion made by Sánchez and Gásquez [26] in the sense that the fluorite structure would not favour the diffusion of the metal atoms into the bulk of oxide supports like ceria.

3.1.3. Final comments and remarks on the nature of the metal/support interaction phenomena in Rh/CeO_2 catalysts

At present, many important questions about the metal/support interaction in Rh/CeO_2 catalysts remain open to discussion. Progress in our current knowledge of such an interaction would be, however, very desirable from both scientific and applied points of view. In particular, an in-depth investigation of its microstructural characteristics is essential in order to arrive at a finer understanding of the general behaviour of Rh/CeO_2 catalysts. First, this would shed some light on what Sánchez and Gásquez [26] called, in a general sense, strong metal/support interaction phenomena. Secondly it would allow us to obtain some further very important data about the deactivation/regeneration mechanisms operating in Rh/CeO_2 catalysts and, by extension, in the so-called TWC's.

The results available from the literature about metal/support interactions in Rh/CeO_2 catalysts are rather contradictory. For catalysts reduced at 773 K and even lower temperatures, some authors have proposed the occurrence of a SMSI-like effect [2,7,62,88]. Their conclusion is mainly based on chemisorption studies, which were carried out by means of different experimental techniques, and catalytic activity data. Though the authors suggest that their catalysts reach a SMSI-like state [2,7,62], they acknowledge some differences of behaviour with respect to the classic Rh/TiO_2 system. In some cases [7,88], no strong inhibition of H_2 chemisorption could be observed, even at the highest reduction temperature (773 K).

We have also investigated the H_2 adsorption and catalytic behaviour of a series of Rh/CeO_2 samples including high surface area/low textural stability (AS) as well as low surface area/high textural stability (BS) ceria supports. Catalysts

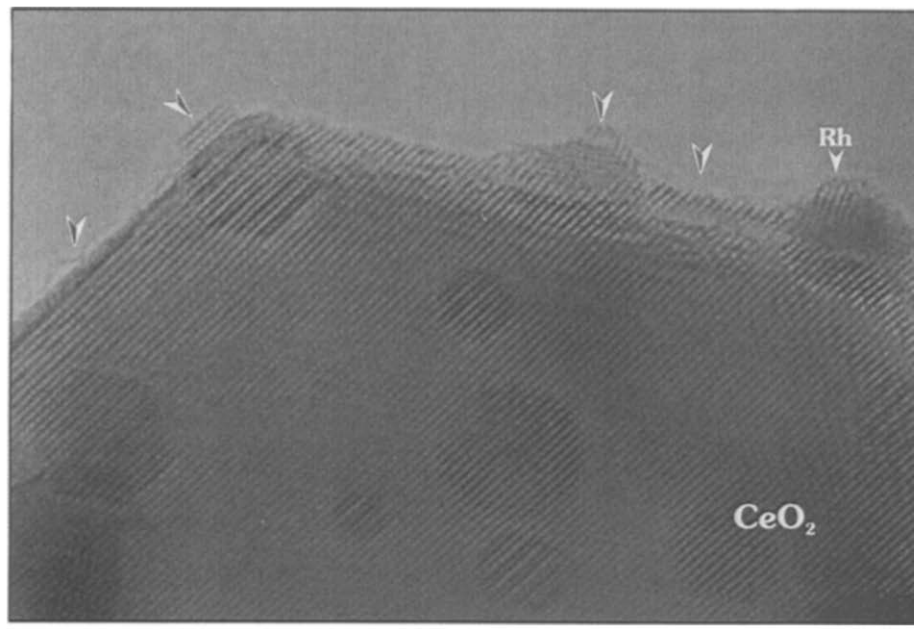

Fig. 15. HREM image of Rh/CeO_2 reduced at 1173 K. Metal particles appear to be covered by the support.

prepared from both $Rh(NO_3)_3$ (N) and $RhCl_3$ (Cl) metal precursors were also studied [20,22,47,50,61]. In the case of N-type catalysts, we have found that the influence of the reduction temperature, either 623 or 773 K, on the amount of chemisorbed hydrogen can be important, but it mainly depends on the textural properties of the corresponding support. The effect of the reduction temperature is far more important in the case of $Rh(N)/CeO_2$-AS catalysts; being almost negligible for $Rh(N)/CeO_2$-BS samples [22,47]. Two major factors are considered to be responsible for the perturbations observed on the chemisorptive properties of $Rh(N)/CeO_2$-AS catalysts, as the reduction temperature was increased from 623 to 773 K [22,47]: the strong sintering undergone by the support, as well as the diminution of the spillover rate at 295 K. This conclusion was reached by carrying out both low temperature (191 K) and high temperature activated hydrogen chemisorption measurements [22,47]. In these latter studies, the hydrogen incorporation to the support was monitored with the help of volumetric adsorption, TPD-H_2, magnetic and electrical conductivity techniques [22].

We have also investigated hydrogen adsorption on a number of $Rh(Cl)/CeO_2$ catalysts [47,50]. Compared to the corresponding $Rh(N)/CeO_2$ catalysts, $Rh(Cl)/CeO_2$ samples show quite different adsorptive properties, thus indicating that chlorine can induce an important perturbation to the chemical properties of these catalysts [50].

If the results reported in refs. [2,7,62,88] are reviewed by taking into account the comments above, some interesting observations can be made. First, some of the catalysts investigated in refs. [2,7,62,88] were prepared from relatively high surface area ceria samples. This implies that some support sintering cannot be excluded, particularly in the case of refs. [7,88], where reduction temperatures as high as 773 K were used. Second, $RhCl_3$ was the metal precursor salt used in all these studies. Therefore, factors other than the intrinsic metal/support interaction phenomena can play an important role in determining the effects observed in refs. [2,7,62,88].

As discussed in [59,77], it is important to separate clearly real metal/support interaction phenomena from other, in principle, indirect effects. In this respect, it should be stressed that all the

results reported in the present work deal with catalysts prepared from $Rh(NO_3)_3$. Also worth noting is that our CeO_2 support is a low surface area sample with relatively high textural stability, so that significant surface area modifications would not be expected, except for the highest reduction temperature, 1173 K. In summary, the ensemble of results obtained from our laboratory suggests that the type of catalyst sample used here is probably the most suitable one to investigate true metal/support interaction phenomena in Rh/CeO_2.

Our HREM study shows that there are two well-defined steps in the microstructural evolution undergone by the Rh/CeO_2 catalysts with the reduction temperature. The first one, up to 773 K, is characterized by the presence of clean and well-faceted rhodium crystallites. From the analysis of a few hundred experimental micrographs, no evidence of metal decoration effects could be obtained. The major microstructural feature consists of the epitaxial growth of Rh(111) planes parallel to $CeO_2(111)$ surface planes. The HREM images in profile view have also shown that this epitaxial relationship is compatible with two different crystallographic orientations of the whole metal crystallite with respect to the support. These two situations have been referred to as $Rh(111)//CeO_2(111)$ 0° and 60°.

In the range of highest reduction temperatures, 973 and 1173 K, the HREM images have clearly shown the occurrence of metal decoration effects. This constitutes the second step in the evolution of the Rh/CeO_2 catalysts. To our knowledge, no HREM studies of Rh/CeO_2 catalysts reduced at such high temperatures have been reported so far. Computer simulation and digital processing techniques were used to confirm that the covering phase consists of ceria. From our study, it could also be concluded that the onset of this effect takes place at a temperature close to 973 K, thus explaining why it was not observed at the reduction temperatures normally reported in the literature, 773 K or lower.

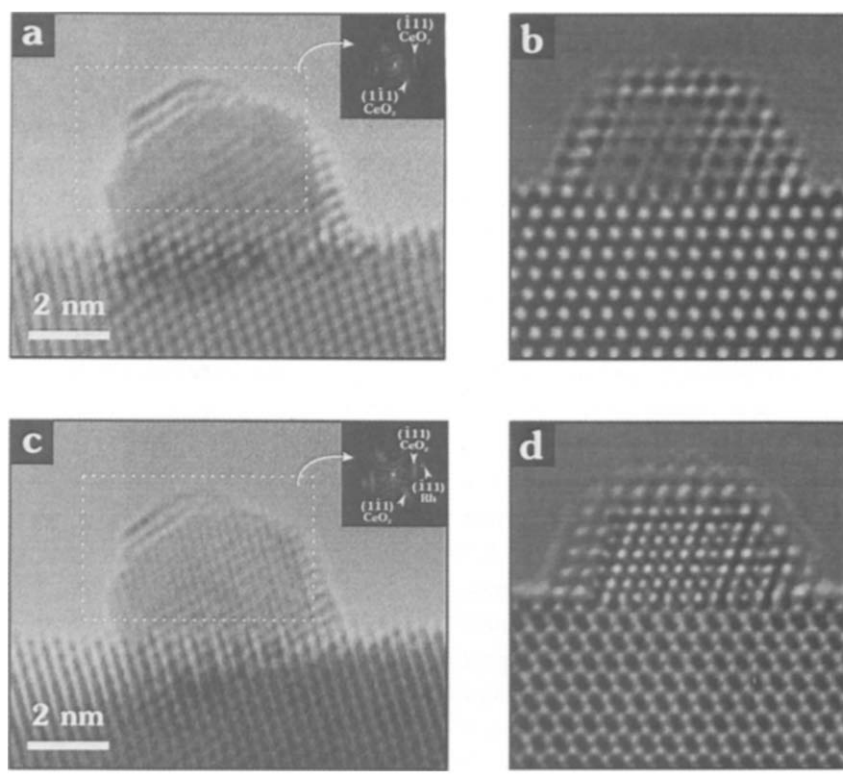

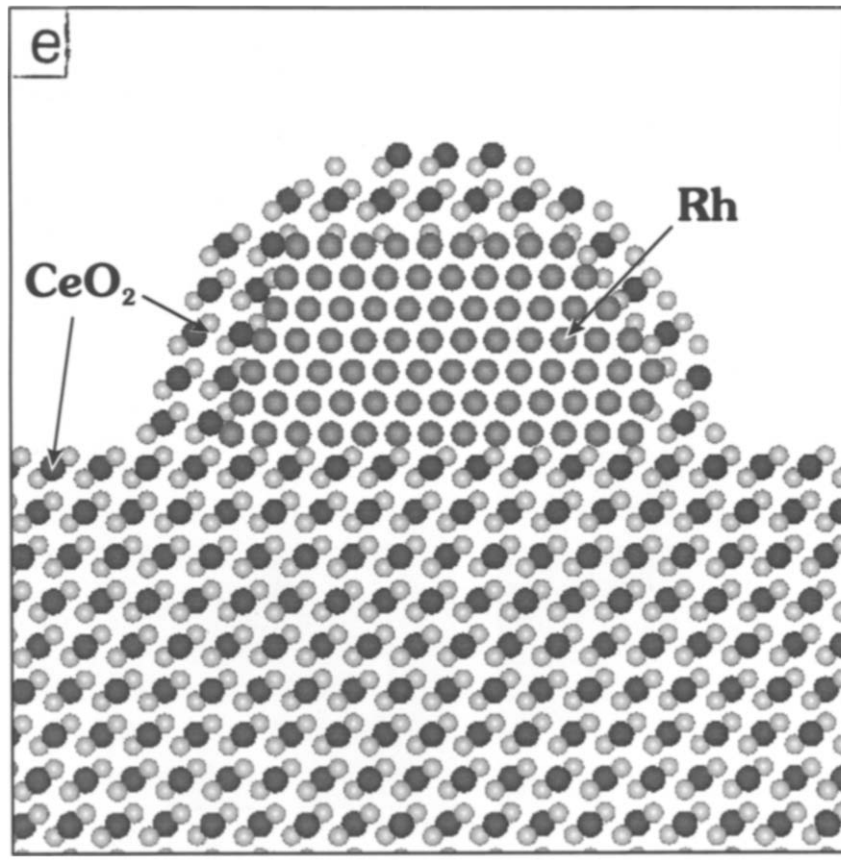

Fig. 16. Experimental and simulated HREM images corresponding to a focal series. The experimental micrographs correspond to Rh/CeO_2 reduced at 1173 K. Computer calculations were based on the structural model shown in (e). Notice resolution change in the metal contrasts as a function of Δf.

The existence of the two steps mentioned above has already been proposed to describe the evolution towards the SMSI state of Rh/TiO_2 catalysts [60]. In this sense, the occurrence of a well-defined structural relationship between rhodium and ceria might be considered as an indication of some electronic interaction between the metal and the support. It should be noted, however, that, in contrast to what is generally observed on Rh/TiO_2 [58–60], our own results [20,22,47,61], as well as some others from the literature [7,88], suggest that a characteristic feature of the Rh/TiO_2 catalysts under the SMSI state, the strong inhibition of H_2 adsorption, is not clearly observed on Rh/CeO_2. In this respect, it is worth mentioning that, on Rh/CeO_2 reduced at 973 K, rhodium can still chemisorb hydrogen [89]. The catalyst studied in ref. [89] is the same investigated in this work. This suggests that either the electronic perturbations induced by ceria are, in general, less important than those observed for titania; or it is a more specific effect. In the latter case, conventional H_2 chemisorption studies would not be the most suitable way of probing the metal/support interactions occurring in Rh/CeO_2.

The discussion above suggests that it would be very desirable to extend the investigation carried out on Rh/CeO_2 to some other noble metals like platinum or palladium. In this way, it would be possible to check the influence of the dispersed metal on the nature of the metal/support interaction phenomena occurring in ceria-containing catalysts.

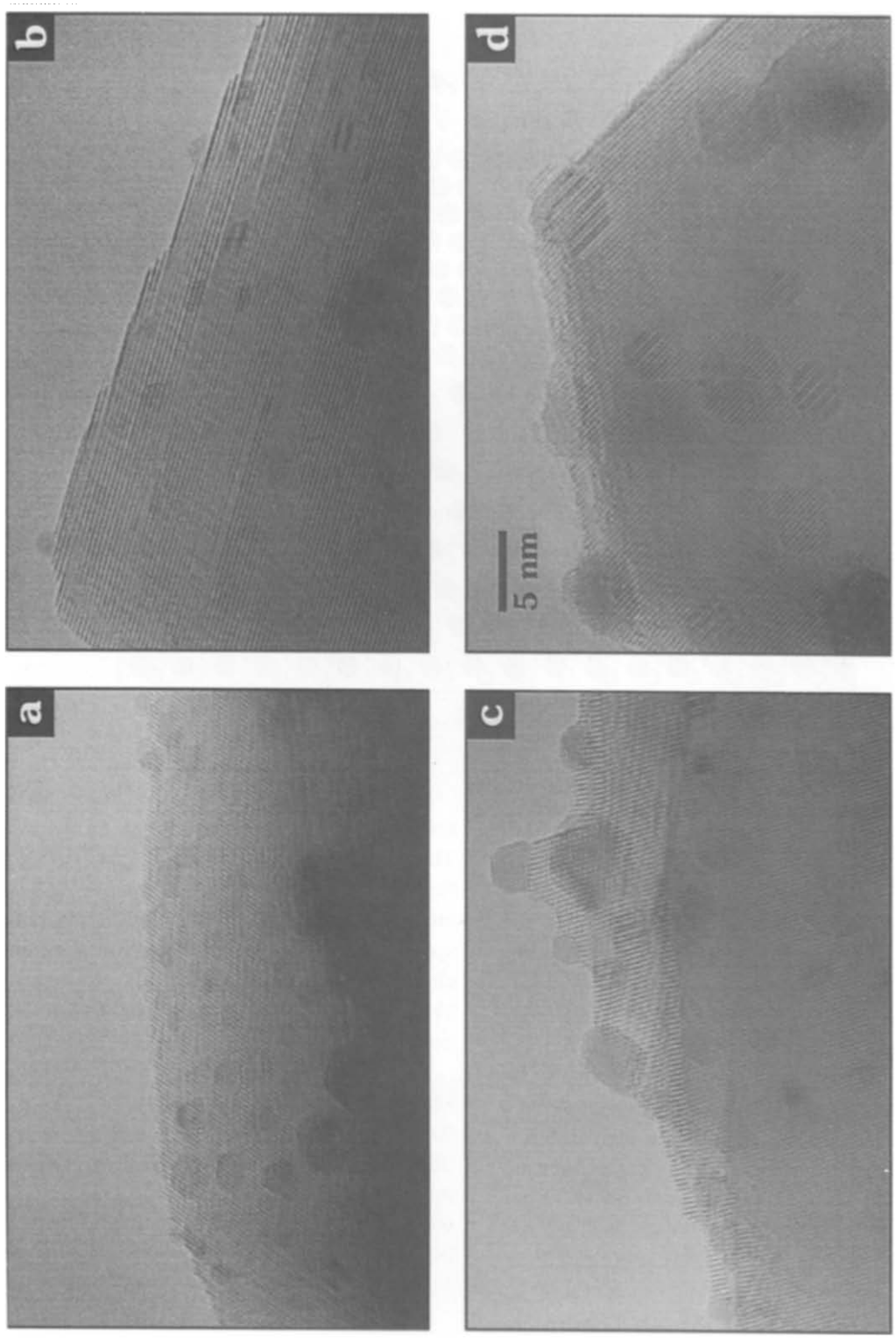

Fig. 17. HREM images of Rh/CeO_2 reduced at 623 K (a), 773 (b), 973 (c) and 1173 (d). Micrographs like those shown here were used to establish the metal particle size distributions reported in Fig. 18.

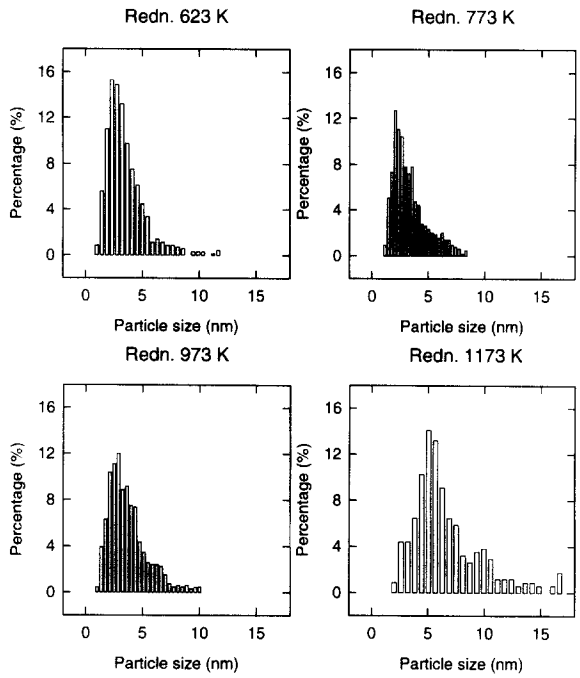

Fig. 18. Metal particle size distributions determined for Rh/CeO_2 reduced at the indicated temperatures.

3.2. Influence of high temperature reduction and reoxidation treatments on metal dispersion in Rh/CeO_2 catalysts. HREM study of the oxidized rhodium phase

It is generally acknowledged that deactivation is a major problem in three-way catalysts [70–72]. Chemical poisoning [72,78], metal sintering [71,72], as well as metal decoration effects like those reported in previous sections of this work, can be considered to be some of the most important factors responsible for the occurrence of this undesirable effect.

The investigation of Rh/CeO_2 model systems can be helpful in understanding the deactivation mechanisms operating in ceria-containing multicomponent catalysts. In the present case, we shall focus our attention on the HREM study of the influence of high temperature reduction and oxidation treatments on the metal dispersion. Likewise, we shall report on the microstructural nature of the oxidized rhodium-containing phases. This microstructural investigation will be complementary to the one carried out on the reduced catalysts, which has been discussed earlier in this work.

By processing some of the experimental HREM micrographs, like those reported in Fig. 17, we have been able to establish the particle size distribution associated with each of the reduced catalysts. Fig. 18 reports on the corresponding distribution curves. In each case, over 200 metal particles were measured. Metal crystallites in profile and planar view were studied. In the first case, the particle size was determined at the metal/support interface. For rhodium crystallites in planar projection, the distance between opposite lateral faces was used to estimate their size.

The distribution profiles in Fig. 18 account for the variation of the percentage of metal particles having a specified size (± 0.25 nm) as a function of the particle size. From them, we could estimate the corresponding mean particle size values. For the catalysts reduced at 623 and 773 K, this value was found to be the same: 3.5 ± 0.2 nm; for the sample reduced at 973 K it was slightly larger: 3.7 ± 0.2 nm; and, finally, for the catalyst reduced at 1173 K, a mean particle size of 6.7 ± 0.6 nm was determined. We can conclude from these results that ceria stabilizes the rhodium particles fairly well up to 973 K, whereas at the highest reduction temperature, 1173 K, an important metal sintering occurs. It should be noted, however, that the distribution curves for the catalysts reduced up to 973 K show some differences, thus suggesting that the metal particle size is not completely insensitive to the reduction temperature, even in the range 623–973 K. It is possible that some growth of the rhodium crystallites at the expense of the smallest, hard to observe, particles may occur.

We have also investigated the effects induced on the metal particles by different thermal treatments in pure oxygen. These treatments were all carried out in a flow of 60 $cm^3\ min^{-1}$. The reduced catalysts were heated from 298 K to the selected oxidation temperature at a rate of 10 K min^{-1}; they were held for 1 h at this temperature, and, finally, they were cooled to 298 K, always in flowing O_2.

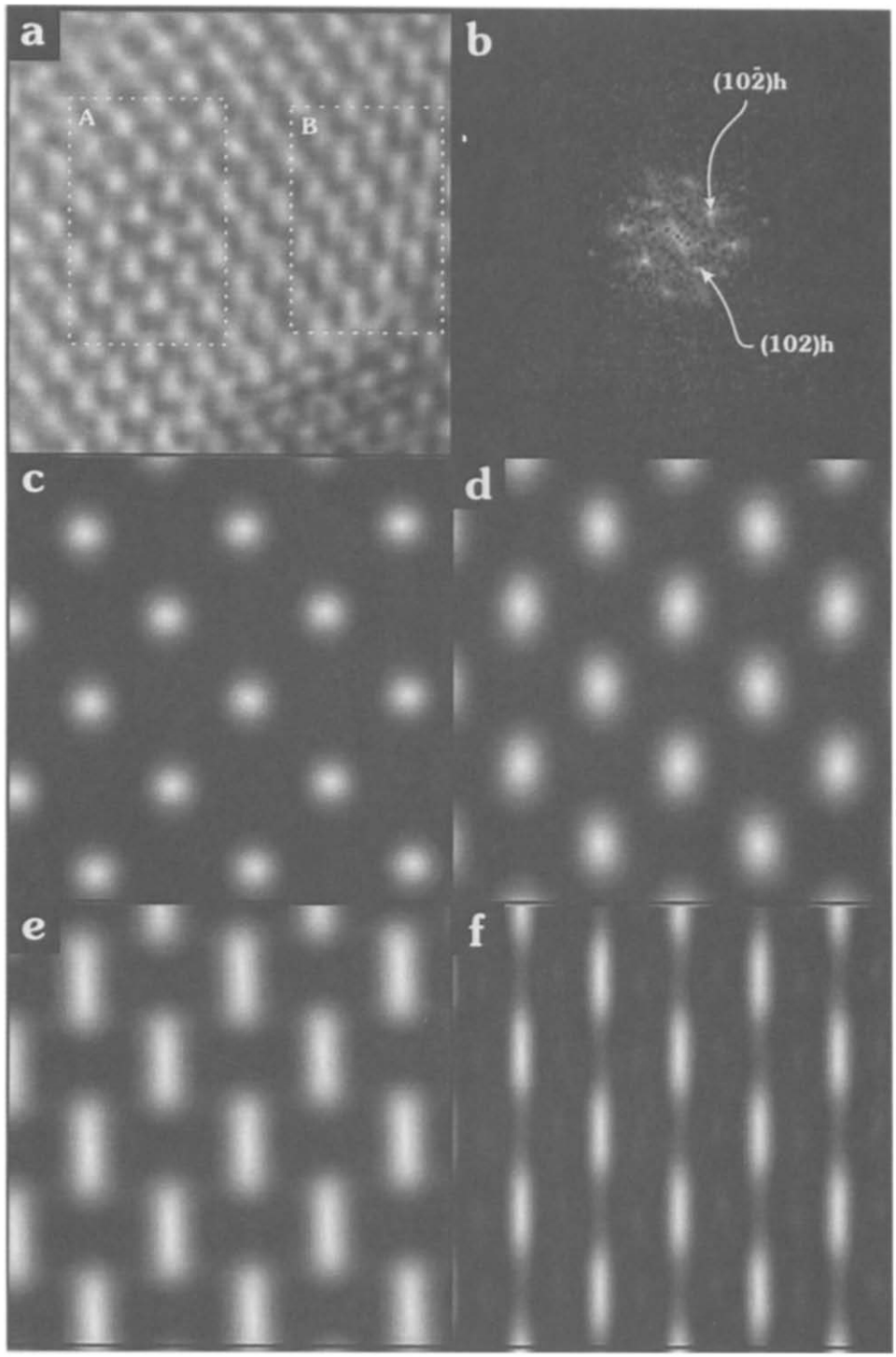

Fig. 19. Experimental and simulated HREM images of Rh_2O_3. (a) Rh/CeO_2 reduced at 973 K and further reoxidized at 773 K, for 1 h (b). (c) and (e) calculated images for hexagonal rhodia. (d) and (f) calculated images for orthorhombic rhodia. Details about the simulation conditions are given in the text.

We shall distinguish the studies carried out on catalysts reduced in the range 623–973 K, from those performed on the sample reduced at 1173 K. In the first case, we have used a single oxidation temperature: 773 K. Several reasons justify the choice of this temperature. A number of authors have used it for reoxidizing supported rhodium catalysts [71,79,80]. Likewise, it is in the range of the oxidation treatments normally applied to recover the supported Rh catalysts from the SMSI state [59,81]. This temperature was also suggested by the quantitative results obtained from a TPO study carried out by us on the same Rh/CeO_2 catalysts investigated here [82]. In accordance with this study [82], the rhodium crystallites would be thoroughly oxidized to Rh_2O_3 upon heating them in O_2(5%)/He at 773 K. This stoichiometry is also in good agreement with that reported by several authors [71,79,80,83,84] from similar studies on supported rhodium catalysts.

Regarding the reoxidation of Rh/CeO_2 reduced at 973 K or below, there are two aspects worth commenting on. The first one deals with the structural properties of the rhodium oxide resulting from this treatment. Three different structures have been reported in the literature for Rh_2O_3 [85]. Two of them, those referred to as I and III in ref. [85], are well characterized from the crystallographic point of view [85,86]. Phase I, with hexagonal corundum-like structure [85,86], has been obtained by thermal decomposition at 873–923 K of a number of rhodium salts [85]. It could also be observed upon oxidation of a rhodium foil, in air, at 873–923 K [87]. Phase III, orthorhombic, with a corundum-related structure [85,86], has also been prepared by direct oxidation in air of metallic rhodium [87]. This latter phase, the most stable one [85,87], was reported to occur after high temperature ($T > 1073$ K) oxidation treatments [86,87]. Likewise, phase III could be identified on Rh/Al_2O_3 catalysts heated in 5% O_2 at 773 K or above [71].

In agreement with that reported earlier for Rh/SiO_2 [80] and Rh/Al_2O_3 [83], heating our Rh/CeO_2 catalyst in O_2 at relatively mild temperatures (773 K) leads to polycrystalline sesquioxide particles [83]. Under these circumstances, the structural identification of the Rh_2O_3 phase present in the sample becomes difficult, because many of the lattice spacings associated to phases I and III are too close to be distinguished easily. Furthermore, the oxidized rhodium particles with sizes below 3–4 nm are unstable under the electron beam. In some cases, Fig. 19, when larger oxide particles are found, a structural analysis is possible. Fig. 19a shows a HREM image corresponding to our Rh/CeO_2 catalyst reduced at 973 K and further oxidized at 773 K. By digital processing of this image, the optical diffraction pattern shown in Fig. 19b could be obtained. This ODP can be interpreted as being due to either orthorhombic Rh_2O_3 in [011] orientation, or to the hexagonal phase in $[2\bar{2}1]$ orientation. As will be discussed below, the latter assignation was chosen in Fig. 19b. In an attempt to arrive at an unambiguous interpretation of Fig. 19a, we have recorded computer-simulated HREM images for both hexagonal and orthorhombic rhodia in the orientations mentioned above. Two series of calculated images were obtained by modifying the sample thickness and defocus. Because of the unusually large size of the oxide particle in Fig. 19a, the sample thickness was varied from 3 to 12 nm. As in the case of the simulations reported earlier in this work, defocus was also varied from 10 to 100 nm. The electronoptical simulation conditions were the same as reported above. Fig. 19c and e account for the calculated images corresponding to the hexagonal phase. They correspond to sample thickness: 9 nm, defocus: 50 nm (Fig. 19c); and sample thickness: 3 nm, defocus: 10 nm (Fig. 19e). Simulated images of orthorhombic rhodia are shown in Fig. 19d (sample thickness: 3 nm, defocus: 20 nm) and 19f (sample thickness: 9 nm, defocus: 20 nm). From the analysis of these simulated images we note that both Fig. 19c and d show contrasts rather similar to those found in region A of the experimental image. In contrast, Fig. 19e shows elongated white contrasts, similar to those observed in region B of Fig. 19a. This type of contrast could not be found in the simulated image for the ortho-

rhombic phase. Though the evidence can be considered rather weak, we suggest that hexagonal rhodia is the phase responsible for the image reported in Fig. 19a. This interpretation is also consistent with the results reported in the literature [85,86], in accordance with which, this phase will probably occur at the mildest oxidation conditions.

We have also checked the effect of the reoxidation treatment on the metal dispersion. For catalysts reduced at temperatures ranging from 623 to 973 K, further oxidized at 773 K, and finally

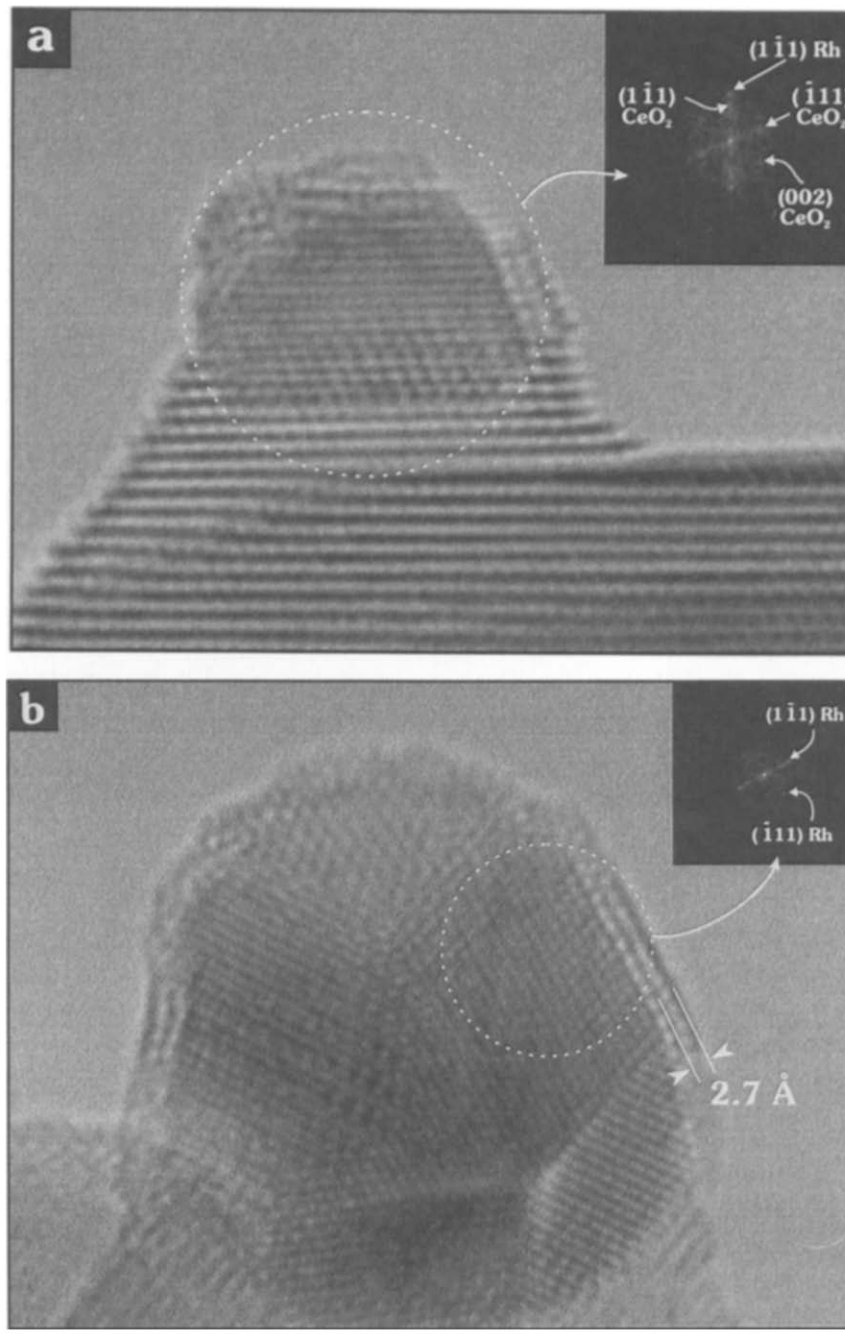

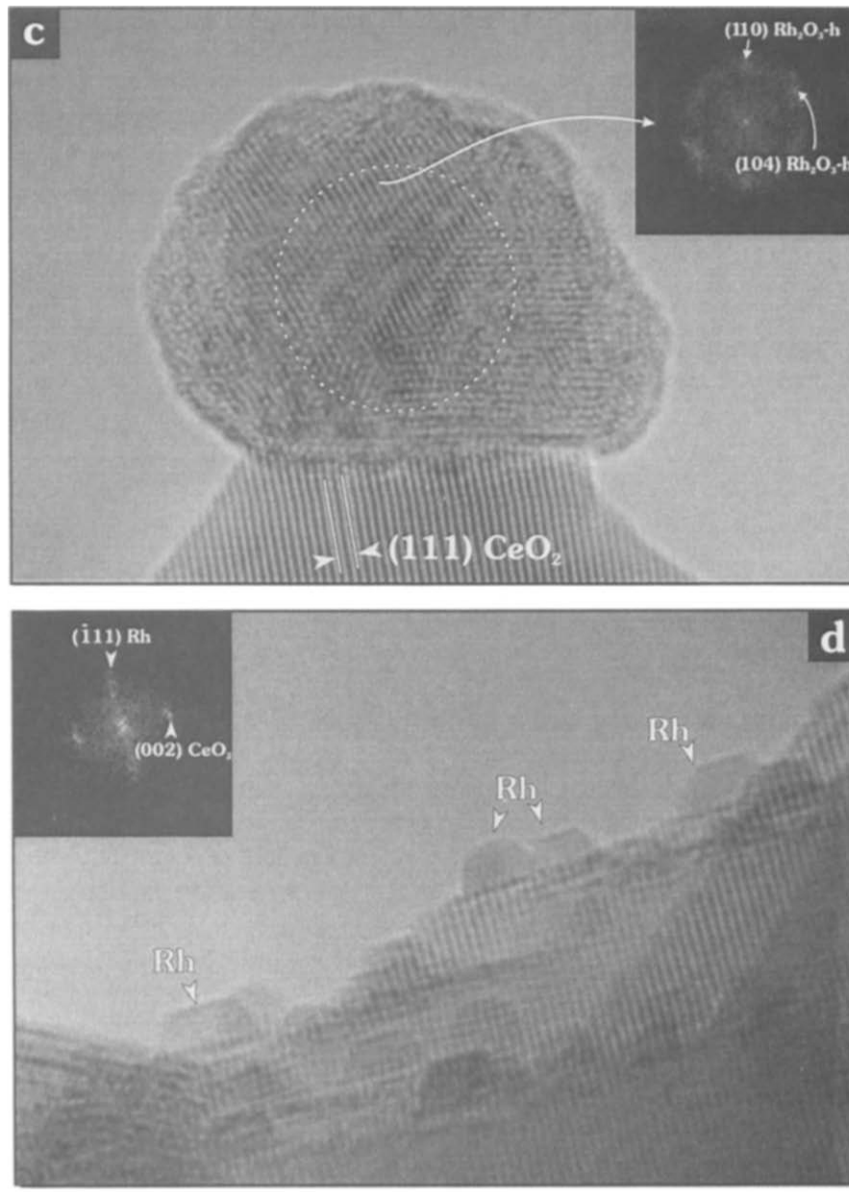

Fig. 20. HREM images corresponding to Rh/CeO_2 reduced at 1173 K and further reoxidized at 373 K (a), 523 K (b), 773 K (c) and 1173 K (d). In the latter case (d) the oxidized phase was reduced under the electron beam.

re-reduced at 623 K, or under the electron beam, the metal particle size distributions show no significant modification of the initial distribution. Therefore, it can be concluded that heating in oxygen, for 1 h, at 773 K, does not induce the redispersion of the rhodium particles supported on ceria.

Since metal decoration was found to be very important on the catalyst reduced at 1173 K, we carried out a more detailed reoxidation study. Oxygen treatments at 373, 523, 773, and 1173 K were performed. Fig. 20 shows representative HREM images for the whole series of treatments mentioned above.

There are a number of aspects to be commented on in relation to Fig. 20. For the mildest oxidation treatments, (373 and 523 K, Fig. 20a and b), the metallic rhodium can easily be identified. Likewise, these HREM images suggest that the phase decorating the metal crystallites is still present. In

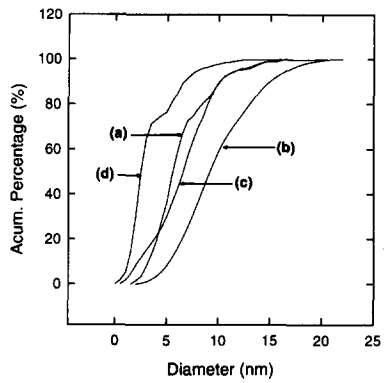

Fig. 21. Rhodium particle size distributions determined from the HREM study of: (a) Rh/CeO_2 reduced at 1173 K; (b) sample (a) reoxidized at 773 K; (c) sample (b) re-reduced at 623 K; (d) sample (a) reoxidized at 1173 K and further reduced 'in situ' by the electron beam.

addition to this, the encircled area in Fig. 20b shows the existence of a few layers of thick phase epitaxially grown on the metal. The fringe spacing for this phase, 0.27 nm, is close to that reported in ref. [79] for a partially oxidized rhodium particle resulting from a similar O_2 treatment. In ref. [79], this lattice spacing value is interpreted as being due to metastable rhodium oxide, with a stoichiometry of RhO. It should be noted, however, that Rh_2O_3 also shows a diffraction line at 0.26 nm [86]. Accordingly, the assignation of these lattice fringes to rhodium sesquioxide should not, in principle, be excluded. In any case, the TPO diagrams recorded in ref. [82] for our Rh/CeO_2 catalysts indicate that the oxidation of the rhodium crystallites starts at around 473 K. Therefore, it seems possible that some oxidized rhodium phase is observed in Fig. 20b.

The oxidation at 773 K of the catalyst reduced at 1173 K leads to the formation of big rounded particles, Fig. 20c. As deduced from our HREM study, the oxidized particles resulting from this treatment consist of polycrystalline rather than disordered material. This is also confirmed by the diffuse optical diffraction pattern recorded for them.

The highest reoxidation temperature, 1173 K, induces a very important change in the microstructure of the rhodium oxide. It spreads over the ceria surface, thus creating an amorphous layer a few ångströms thick which is rapidly reduced under the electron beam. As a result, the ceria surface becomes covered by small crystalline rhodium particles. The evolution of the rhodium oxide under the electron beam was fast enough so that it was difficult to obtain images of the oxidized phase. Fig. 20d shows the metal crystallites formed 'in situ' by reduction of the initial amorphous rhodium oxide.

Fig. 20d clearly suggests that the metal particles resulting from the reduction under the electron beam are much smaller than those observed on the catalyst reduced at 1173 K. This indicates that the high temperature reoxidation induces the redispersion of the metal phase. To confirm this, we have studied the evolution of the particle size distribution of rhodium throughout the series of oxidation/reduction treatments applied to the catalyst previously reduced at 1173 K. Fig. 21, in which integral distribution curves are plotted, summarizes the results obtained from this study. Fig. 21a shows the curve obtained for the initial catalyst (reduction temperature: 1173 K). As deduced from Fig. 21b, the treatment in O_2 at 773 K causes a strong shift of the distribution curve. The mean particle size associated with this curve was found to be 10.0 nm. This observation is consistent with the lattice expansion inherent to the formation of the rhodium sesquioxide. Upon further reduction at 623 K of the sample reoxidized at 773 K, we obtain curve c. In good agreement with that observed on catalysts reduced up to 973 K, the particle size distribution depicted in Fig. 21c suggests that the reoxidation treatment at 773 K does not induce a strong redispersion of the rhodium. In effect, the comparison of curves a and c in Fig. 21 suggests that redispersion is rather modest. In fact, the mean particle size determined from the distribution plotted in Fig. 21c is 6.8 nm which is very similar to that estimated for the initial catalyst reduced at 1173 K. In contrast to this, the reoxidation treatment at 1173 K, as presumed, causes a rather strong decrease of the metal crystal size, the mean value of which is 3.6 nm, which is very close to that determined by direct reduction, at 623 K, of the $Rh(NO_3)_3/CeO_2$ precursor system.

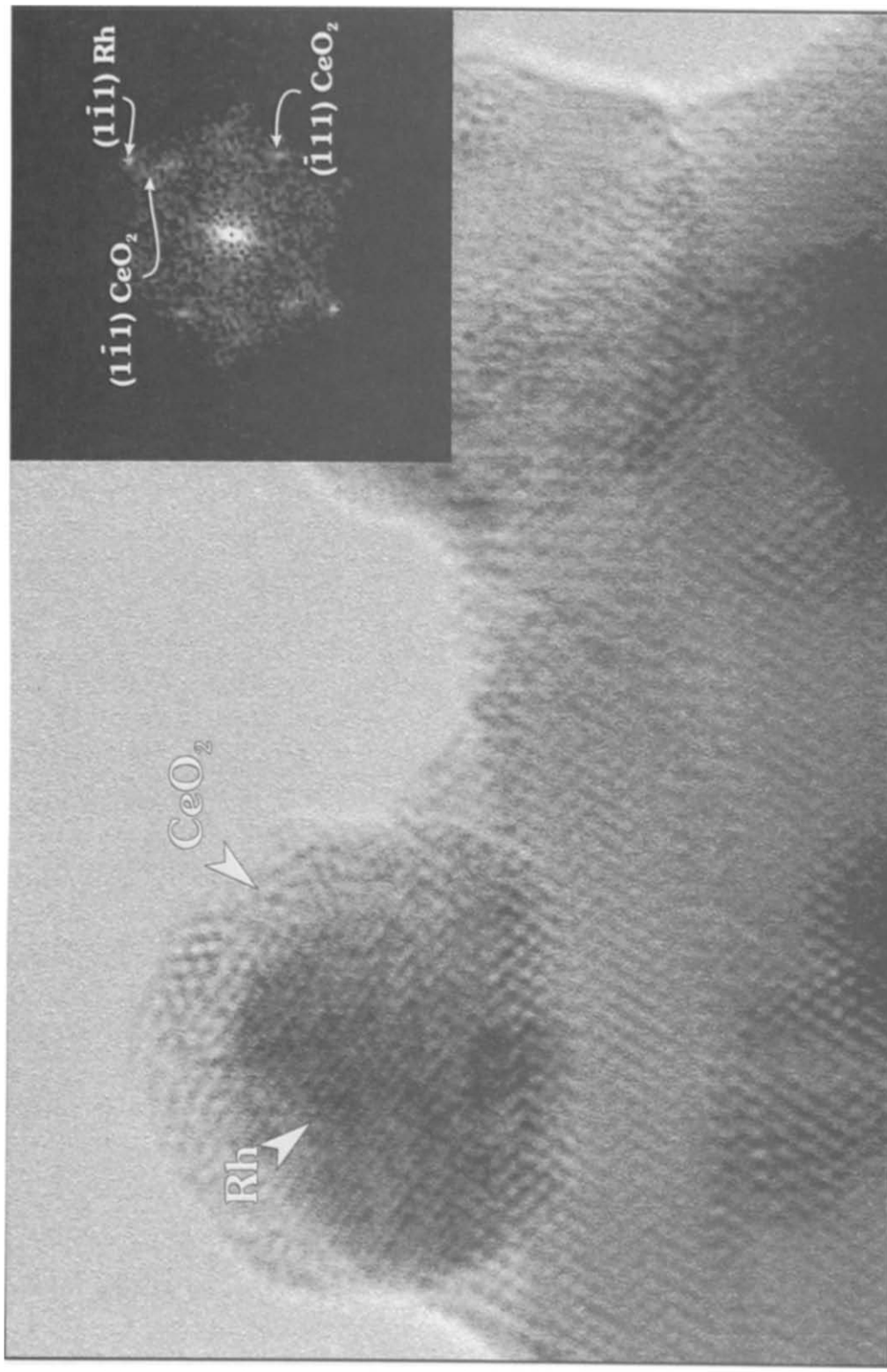

Fig. 22. HREM image of Rh/CeO_2 reduced at 1173 K, further reoxidized at 773 K, for 1 h, and finally reduced with H_2 at 623 K. Notice that the metal particle is not recovered from the decoration effect.

Finally, our HREM study provided some further information about the conditions required to completely recover the Rh/CeO_2 catalysts from the metal decoration effects. We have already mentioned that the milder O_2 treatments, 373 and 523 K, do not eliminate the support phase covering the rhodium particles, Fig. 21a and b. In contrast, the reduction of the catalyst reoxidized at 1173 K leads to well-faceted, perfectly clean metal particles. We have also studied, the effect of the reoxidation treatment at 773 K. It is known that, in the case of Rh/TiO_2 catalysts, this temperature is high enough to recover the catalysts from the SMSI state [59,81]. Fig. 22 shows a HREM image corresponding to our Rh/CeO_2 catalyst reduced at 1173 K, reoxidized at 773 K and finally re-reduced at 623 K, as usual, in a flow of H_2. We note that the metal particles continue to be decorated, thus suggesting that the reoxidation treatment at 773 K does not ensure the complete elimination of the covering phase. There are some other interesting conclusions which we can draw from this observation. It seems likely that the oxide formed at 773 K actually consists of a cerium-containing phase, the segregation of ceria requiring higher oxidations temperatures. Therefore, the onset of the metal decoration effect as well as its recovery require harder thermal treatments than those needed in the case of the classic Rh/TiO_2 system. This can be considered as an important feature in connection with the deactivation/regeneration processes in ceria-supported rhodium catalysts.

Acknowledgements

This work received financial support from the DGICYT (Project: PB92-0483) and the Junta de Andalucía. We are very grateful to Dr. P. Stadelman for his kind help in installing the EMS software package and subsequent training. The HREM images reported here were obtained at the Electron Microscopy Facilities of UCA. We acknowledge Johnson Matthey for a loan of noble metals. We thank Mrs. G. Blanco for her contribution to the preparation of the figures included in this work.

References

[1] J. El Fallah, S. Boujana, H. Dexpert, A. Kiennemann, J. Majerus, O. Touret, F. Villain and F. Le Normand, J. Phys. Chem., 98 (1994) 5522.
[2] J. Cunningham, D. Cullinane, J. Sanz, J.M. Rojo, J.A. Soria and J.L.G. Fierro, J. Chem. Soc., Faraday Trans., 88 (1992) 3233.
[3] M. Primet, M. El Azhar, R. Frety and M. Guenin, Appl. Catal., 59 (1990) 153.
[4] J.L. Duplan and H. Praliaud, Appl. Catal., 67 (1991) 325.
[5] J.P. Holgado and G. Munuera, in A. Frennet and J.M. Bastin (Editors), Preprints CAPoC-3, Vol. 2, Brussels, 1994, pp. 1–12.
[6] J. Soria, A. Martínez-Arias and J.C. Conesa, Vacuum, 43 (1992) 437.
[7] A. Trovarelli, G. Dolcetti, C. Leitenburg, J. Kaspar, P. Finetti and A. Santoni, J. Chem. Soc., Faraday Trans., 88 (1992) 1311.
[8] E.A. Shaw, A.P. Walker, T. Rayment and R.M. Lambert, J. Catal., 134 (1992) 747.
[9] J.C. Lavalley, J. Saussey, J. Lamotte, R. Breault, J.P. Hindermann and A. Kiennemann, J. Phys. Chem., 94 (1990) 5941.
[10] F. Le Normand, L. Hilaire, K. Killi, G. Kril and G. Maire, J. Phys. Chem., 92 (1988) 2561.
[11] C. Binet, A. Jadi, J.C. Lavalley and M. Boutonet-Kizling, J. Chem. Soc., Faraday Trans., 88 (1992) 2079.
[12] J. Barrault, A. Alouche, V. Paul-Boncour, L. Hilaire and A. Percheron-Guegan, Appl. Catal., 46 (1989) 269.
[13] D. Martin and D. Duprez, Stud. Surf. Sci. Catal., 77 (1993) 201.
[14] H.D. Cochrane, J.L. Hutchinson, D. White, G.M. Parkinson, C. Dupas and A.J. Scott, Ultramicroscopy, 34 (1990) 10.
[15] E. Ramaroson, J.F. Tempere, M.F. Gilleux, F. Vergand, H. Roulet, D. Dufour, J. Chem. Soc., Faraday Trans., 88 (1992) 1211.
[16] A.A. Kaïs, A. Benami, C.F. Aïsi, G. Wrobel and M. Guelton, J. Chem. Soc., Faraday Trans., 88 (1992) 1321.
[17] A. Bensalem, G. Shafeev and F. Bozon-Verduraz, Catal. Lett., 18 (1993) 165.
[18] S. Bernal, F.J. Botana, R. García, Z. Kang, M.L. López, M. Pan, F. Ramírez and J.M. Rodríguez-Izquierdo, Catal. Today, 2, (1988) 653.
[19] S. Bernal, F.J. Botana, G.A. Cifredo, J.J. Calvino, R. García and J.M. Rodríguez-Izquierdo, Ultramicroscopy, 34 (1990) 60.
[20] S. Bernal, G.A. Cifredo, J.J. Calvino, J.M. Rodríguez-Izquierdo, V. Perrichon and A. Laachir, J. Chem. Soc., Chem. Commun., (1992) 460.
[21] S. Bernal, G.A. Cifredo, J.J. Calvino, J.M. Rodríguez-Izquierdo, V. Perrichon and A. Laachir, J. Catal., 137 (1992) 1
[22] S. Bernal, J.J. Calvino, G.A. Cifredo, A. Laachir, V. Perrichon and J.M. Herrmann, Langmuir, 10 (1994) 717.

[23] L. Mendelovici and M. Steinberg, J. Catal., 96 (1985) 285.
[24] J.C. Summers and S.A. Ausen, J. Catal., 58 (1979) 131.
[25] J.R. Katzer, A.W. Sleight, P. Gajardo, M. Edwar, F. Gleason and S. Mc Millan, Discuss. Faraday Soc., 72 (1982) 121.
[26] M.G. Sánchez and J.L. Gázquez, J. Catal., 104 (1987) 120.
[27] M. Pan, J.M. Cowley and R. García, Micron Microscopica Acta, 18 (1987) 165.
[28] T. Jin, T. Okuhara, G.J. Mains and M. White, J. Phys. Chem., 91 (1987) 3310.
[29] T. Jin, Y. Zhou, G.J. Mains and J.M. White, J. Phys. Chem., 91 (1987) 5931.
[30] Y. Zhou, M. Nakashima and J.M. White, J. Phys. Chem., 92 (1988) 812.
[31] D.W. Daniel, J. Phys. Chem., 92 (1988) 3891.
[32] B.K. Cho, J. Catal., 131 (1991) 74.
[33] L.L. Murrell, S.J. Tauster and D.R. Anderson, in A. Crucq (Editor), Proceedings CAPoC-2, Elsevier, Amsterdam, 1991, pp. 275–289.
[34] D. Kalakkad, A.K. Datye and H. Robota, Appl. Catal. B: Environmental, 1 (1992) 191.
[35] G.S. Zafiris and R.J. Gorte, J. Catal., 139 (1993) 561.
[36] J. Cunningham, D. Cullinane, F. Farrell, M.A. Morris, A.K. Datye and D. Kalakkad, in A. Frennet and J.M. Bastin (Editors), Preprints CAPoC-3, Vol. 2, Brussels, 1994, pp. 107–117.
[37] K.C. Taylor, Catal. Rev. Sci. Eng., 35 (1993) 457
[38] B. Harrison, A.F. Diwell and C. Hallet, Platinum Met. Rev., 32 (1988) 73.
[39] P. Lööf, B. Kasemo and K.E. Keck, J. Catal., 118 (1989) 339.
[40] G. Kim, Ind. Eng. Chem. Prod. Res. Dev., 21 (1982) 267.
[41] J.L.G. Fierro, J. Soria, J. Sanz and J.M. Rojo, J. Solid State Chem., 66 (1987) 154.
[42] A. Laachir, V. Perrichon, A. Badri, J. Lamotte, E. Catherine, J.C. Lavalley, J. El Fallah, L. Hilaire, F. Le Normand, E. Quéméré, G.N. Sauvion and O. Touret, J. Chem. Soc., Faraday Trans., 87 (1991) 1601.
[43] S. Bernal, J.J. Calvino, G.A. Cifredo, J.M. Gatica, J.A. Pérez Omil and J.M. Pintado, J. Chem. Soc., Faraday Trans., 89 (1993) 3499.
[44] A. Badri, J. Lamotte, J.C. Lavalley, A. Laachir, V. Perrichon, O. Touret, G.N. Sauvion and E. Quéméré, Europ. J. Solid State Chem., 28 (1991) 445.
[45] C. Li, Y. Sakata, T. Arai, K. Domen, K. Maruya and T. Onishi, J. Chem. Soc., Faraday Trans. I, 85 (1989) 929.
[46] C. Li, Y. Sakata, T. Arai, K. Domen, K. Maruya and T. Onishi, J. Chem. Soc., Faraday Trans. I, 85 (1989) 1451.
[47] S. Bernal, F.J. Botana, J.J. Calvino, M.A. Cauqui, G.A. Cifredo, A. Jobacho, J.M. Pintado and J.M. Rodríguez-Izquierdo, J. Phys. Chem., 97 (1993) 4118.
[48] M. Wolcyrz and L. Kepinski, J. Solid State Chem., 99 (1992) 409.
[49] S. Bernal, F.J. Botana, J.J. Calvino, G.A. Cifredo and J.A. Pérez Omil, Proceedings of EMAG-93, Inst. Phys. Conf. Ser. No. 138, Liverpool (1993), pp. 485–488.
[50] S. Bernal, J.J. Calvino, G.A. Cifredo, J.M. Gatica, J.A. Pérez Omil, A. Laachir and V. Perrichon, in A. Frennet and J.M. Bastin (Editors), Preprints CAPoC-3, Vol. 2, Brussels, 1994, pp. 275–283.
[51] H. Abderrahim and D. Duprez, in M.J. Phillips and M. Ternan (Editors), Proc. 9th. Int. Cong. Catal., Vol. 3, Ottawa, Canada, 1988, p. 1296.
[52] K. Otsuka, M. Hatano and A. Morikawa, React. Solids, 1 (1983) 87.
[53] V. Perrichon, A. Laachir, G. Bergeret, R. Frety, L. Tournayan and O. Touret, J. Chem. Soc., Faraday Trans., 90 (1994) 773.
[54] P. Meriaudeau, J.F. Dutel, M. Dufaux and C. Naccache, Stud. Surf. Sci. Catal., 11 (1982) 95.
[55] P. Meriaudeau, M. Dufaux and C. Naccache, in Strong Metal/Support Interactions, ACS Symp. Ser., 298 (1986) 118–122.
[56] M. Guenin, P.N. Da Silva and R. Frety, Appl. Catal., 27 (1986) 313.
[57] G. Munuera, A. Fernández and A.R. González-Elipe, in A. Crucq (Editor), Proceedings of CAPoC-2, Elsevier, Amsterdam, 1991, pp. 207–219.
[58] S.J. Tauster, Acc. Chem. Res., 20 (1987) 389.
[59] G.L. Haller and D.E. Resasco, Adv. Catal., 36 (1989) 173.
[60] J.P. Belzunegui, J. Sanz and J.M. Rojo, J. Am. Chem. Soc., 114 (1992) 6749.
[61] S. Bernal, J.J. Calvino, M.A. Cauqui, G.A. Cifredo, A. Jobacho and J.M. Rodríguez-Izquierdo, Appl. Catal. A: General, 99 (1993) 1.
[62] J. Cunningham, S. O'Brien, J. Sanz, J.M. Rojo, J. Soria and J.L.G. Fierro, J. Mol. Catal., 57 (1990) 379.
[63] M. Pan, R. García, D.J. Smith, J.M. Cowley, and G.A. Cifredo, in G.W. Bailey (Editor), Proceedings 47th Meeting of the Electron Microscopy Society of America, San Francisco Press, San Francisco, 1989, pp. 256–257.
[64] M. Pan, Ph.D. Thesis, Arizona State University (1991).
[65] T. Chojnacki, K. Krause and L.D. Schmidt, J. Catal., 128 (1991) 161.
[66] K.R. Krause, P. Schabes-Retchkiman and L.D. Schmidt, J. Catal., 134 (1992) 204.
[67] J.M. Schwartz and L.D. Schmidt, J. Catal., 138 (1992) 283.
[68] A.D. Logan, E.J. Braunschweig, A.K. Datye and D.J. Smith, Langmuir, 4 (1988) 827.
[69] A.K. Singh, N.K. Pande and A.T. Bell, J. Catal., 94 (1985) 422.
[70] D.D. Beck and C.J. Carr, J. Catal., 144 (1993) 296.
[71] D.D. Beck, T.W. Capehart, C. Wong and D.N. Belton, J. Catal., 144 (1993) 311.
[72] B.J. Cooper, Platium Metals Rev., 38 (1994) 2.
[73] A.K. Datye and D.J. Smith, Catal. Rev. Sci. Eng., 34 (1992) 129.
[74] S. Giorgio, C.R. Henri, C. Chapon and G. Nihoul, in A. López and M.I. Rodríguez (Editors), Proceedings of EUREM-92, Vol. 2, Granada (1992), p. 645.
[75] J.P. Eberhart, Structural and Chemical Analysis of Materials. Ch. 19, John Wiley, New York, 1991, p. 422.
[76] L. Reimer, Transmission Electron Microscopy, Springer Verlag, Berlin, 1984, p. 335.
[77] G.C. Bond and R. Burch, Catalysis (London), 6 (1983) 27.
[78] G. Kim, M.V. Ernest and S.R. Montgomery, Ind. Eng. Chem. Prod. Res. Dev., 23 (1984) 525.
[79] A.D. Logan, E.J. Braunschweig and A.K. Datye, Ultramicroscopy, 31 (1989) 132.
[80] A.D. Logan, K. Sharoudi and A.K. Datye, J. Phys. Chem., 95 (1991) 5568.

[81] J.P. Belzunegui, J.M. Rojo and J. Sanz, J. Phys. Chem., 95 (1991) 3463.
[82] S. Bernal, G. Blanco, J.J. Calvino, G.A. Cifredo, J.A. Pérez Omil, J.M. Pintado and A. Varo, In C. Cortés and S. Vic (Editors), Proceedings of the II World Congress, 'New Developments in Selective Oxidation', Elsevier, Amsterdam, 1994, pp. 507–514.
[83] C. Wong and R.W. McCabe, J. Catal., 107 (1987) 535.
[84] J. Burkhardt and L.D. Schmidt, J. Catal., 116 (1989) 240.
[85] A. Wold and K. Dwight, Solid State Chemistry, Chapman and Hall, New York, 1993, p. 117.
[86] A. Wold, R.J. Arnott and W.J. Croft, Inorg. Chem., 2 (1963) 972.
[87] L.A. Carol and G.S. Mann, Oxidat. Metals, 34 (1990) 1.
[88] A. Trovarelli, C. Leitenburg and G. Dolcetti, J. Chem. Soc., Chem. Commun., (1991) 472.
[89] S. Bernal and J.M. Pintado, unpublished results.